Journal of Medical Ultrasound (2012) **20**, 8—31

Available online at www.sciencedirect.com

SciVerse ScienceDirect

journal homepage: www.jmu-online.com

REVIEW ARTICLE

Capacitive Micromachined Ultrasonic Transducers: Technology and Application

Muhammed Sabri Salim [1]*, M.F. Abd Malek [2], R.B.W. Heng [1], K.M. Juni [3], Naseer Sabri [4]

[1] *School of Mechatronics Engineering,* [2] *School of Electrical System Engineering,* [3] *Electrical Eng. Dept. Politeknik Tuanku Syed Sirajuddin, and* [4] *School of Computer & Communication Engineering, University Malaysia Perlis, Kangar, Malaysia*

Received 22 July, 2011; accepted 9 February, 2012

KEY WORDS
capacitive micromachined ultrasonic transducer,
fabrication,
image sensor,
ultrasonography

Capacitive micromachined ultrasonic tranducers (cMUTs) have recently emerged as an alternative to conventional piezoelectric transducers. They offer many advantages in terms of bandwidth, fabrication of layer arrays, efficiency, and sensitivity. This research presents the principles of operation, fabrication process steps, and application of the capacitive micromachined ultrasound transducer. The study also demonstrates in detail the collapse voltage design parameter of a cMUT membrane. Several important applications are presented to show the feasibility of using cMUTs which are demonstrated by imaging examples in immersion and air due to the cMUT capability of producing large bandwidth (123% fractional bandwidth) and lower impedance mismatch. Finally, the advantages of three-dimensional echographic images based on moving ultrasound linear array its technique are discussed in detail and compared with those of two-dimensional optical hand geometry.

Introduction

Piezoelectric crystals, ceramics, polymers, and piezocomposite materials have long dominated ultrasonic transducer technology, especially in medical ultrasound imaging. In recent years, thanks to advances in microfabrication techniques, the technology of capacitive micromachined ultrasonic transducers (cMUTs) has emerged as a competitive technology in the field of medical imaging.

The principle of operation is the well-known electrostatic transduction mechanism. The basic element of a cMUT is a capacitor cell with one fixed electrode (back plate) and a second one supported by a flexible membrane that can vibrate. If an alternating voltage is superimposed on the bias voltage, applied between the membrane and

* Correspondence to: Dr Muhammed S. Salim, School of Mechatronics Eng. UniMAP, Kangar 01000, Malaysia.
E-mail addresses: muhsabri1967@yahoo.com, muhdeli@yahoo.com (M.S. Salim).

0929-6441
doi:10.1016/j.jmu.2012.02.001

the back plate, the modulation of the electrostatic force results in the vibration of the membrane with subsequent generation of ultrasonography at the same frequency of the modulation. Conversely, when the biased membrane is subjected to an incident ultrasonic wave, a change of capacitance, due to membrane vibration, can be detected. The idea of generating acoustic waves utilizing the electrostatic attraction force between the plates of a condenser is as old as the early piezoelectric transducers [1]. However, only in the early 1990s did the development of micromachining technology allow for the fabrication of electrostatic transducers consisting of a large number of membranes with precisely controlled dimensions in the order of tens of microns for operation in the megahertz (mHz) range [2]. The electrode separation with this technology can be made very narrow, in the submicron range, enabling high electric fields inside the gap that result in high transduction efficiency and sensitivity.

cMUTs are fabricated onto silicon wafers by means of silicon micromachining techniques, using standard integrated circuits (IC) fabrication processes. This makes possible the realization of large one- and two-dimensional (2-D) transducer arrays by choosing the proper photolithographic masks. 2-D arrays with a large number of elements are suitable for real-time three-dimensional (3-D) medical imaging, which is an important topic of current research. There are two main limitations in designing volumetric imaging systems with conventional 2-D piezoelectric arrays: (1) the low acoustic power output and the receiver sensitivity because of the small size of the elements; and (2) the difficulty in providing individual electrical connections to each element [3]. cMUT technology has proved to be a good candidate to overcome these challenges, and the first 2-D cMUT arrays having 128 $\times$ 128 elements, electrically connected by through-wafer interconnects, have been successfully fabricated and characterized [4].

Other important advantages of cMUTs, compared with current piezoelectric transducers, are the wider immersion bandwidth that results in improved image resolution, low noise, and the potentiality to be integrated with electronic circuits on the same wafer. The broad bandwidth of cMUTs also enables other imaging modalities, such as tissue harmonic imaging, in which energy is transmitted at a fundamental frequency, and an image is formed with the energy at the second harmonic [5]. The cMUTs are also promising for high-frequency applications, such as intravascular ultrasound imaging (IVUS). Other potential applications include air-coupled non-destructive evaluation [6], ultrasonic flow meters for narrow gas pipelines [7], microphones with RF detection [8], Lamb wave devices [9], and smart microfluidic channels [10].

This review is divided into three sections. The first section focuses on the principles of operation and modeling of electrostatic transducers. The second section gives an overview of the fabrication processes developed in the past decade to manufacture cMUTs, and addresses process issues, such as choice of materials for process compatibility and reliability. The third section winds up with a description of the potential applications of cMUTs, of which medical imaging has been successfully demonstrated [11–70].

Principles of operation

The electrostatic force generated on the plates of a capacitor is proportional to the square of the applied voltage, the area of the capacitor, and the permittivity of the material between the plates, and inversely proportional to the square of the separation between the plates:

$$F_{elec}=\frac{\varepsilon_o S V^2}{2d^2} \tag{1}$$

where S is the area of capacitor plates, V is the applied bias voltage, ε_o is the permittivity of free space between capacitor plates, and d is the distance between the capacitor plates. Because the electrostatic force is proportional to the square of the bias voltage, linear cMUT operation requires direct current (DC) bias voltage together with the alternating current (AC) voltage ($V = V_{DC} + V_{AC}$). Then, the electrostatic force can be written as:

$$F_{elec}=\frac{\varepsilon_o S}{2d^2}\left(V_{DC}^2+2V_{DC}V_{AC}+V_{AC}^2\right) \tag{2}$$

The first term in parenthesis represents the static force, the second term represents the excitation force proportional to the applied AC voltage, and the last term represents the harmonic contribution of the AC voltage, which also contributes to the static force. When the DC bias voltage is much larger than the AC excitation, the harmonic contribution can be ignored [69].

Collapse voltage calculation

An important design parameter of a cMUT membrane is the collapse voltage; at this voltage, the attractive force can no longer be balanced by the restoring force of the membrane, and the membrane collapses onto the substrate. It is crucial to calculate the collapse voltage accurately since it determines the operating point of the device. Initially, the collapse voltage was calculated by approximating the displacement of the membrane by a piston transducer [11]. In this approach, the piston transducer is assumed to be moving by the same amount of average membrane displacement. The static displacement of the membrane is greatest at the center and reduces close to its rim. Therefore, the average displacement of the membrane is smaller than the displacement at its center. Since the equivalent piston transducer does not move as much as the center of the membrane, the piston transducer approximation results in higher collapse voltage.

More accurate calculation of collapse voltage requires the calculation of membrane displacement profile, which can be achieved by dividing the gap into smaller capacitors. Each capacitor applies an electrostatic force determined by the deflection of the membrane segment where it is attached. Fig. 1 shows a circular membrane and the gap. The gap is composed of many small capacitors. Using the configuration shown in Fig. 1, it is possible to calculate the electrostatic force applied to each segment on the membrane. Note that the segments are circular rings. The electrostatic force on each segment is given by

$$F_{elec}=\frac{\varepsilon_o V_{DC}^2 S_i}{2d_i^2} \tag{3}$$

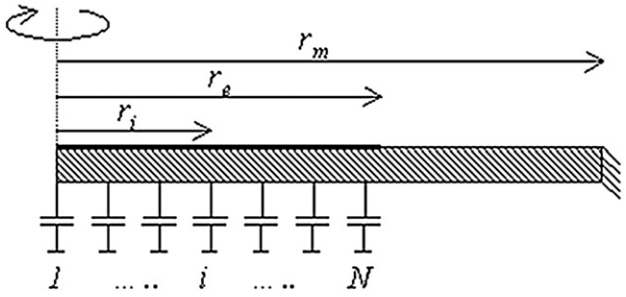

Fig. 1 Membrane and the air gap. The air gap is composed of many parallel capacitors [69].

where V_{DC} is the bias voltage, S_i is the area of the i^{th} capacitor plates, and d_i is the effective gap height (distance) of the i^{th} capacitor plates. The effective gap height can be calculated by

$$d_i = \frac{t_m}{\varepsilon_{r1}} + \frac{t_{ins}}{\varepsilon_{r2}} + g_i \tag{4}$$

where t_m and t_{ins} are the thickness of the membrane and the insulator layer, respectively, whereas g_i is the vacuum gap of the corresponding segment. ε_r is the dielectric constant of the insulating layer or the membrane material.

The corresponding membrane displacement as a result of the electrostatic force over the electrode can be calculated using the plate theorem [12]. Each capacitor applies certain pressure over the small annular segment, as shown in Fig. 1. The total displacement can be found by superposing the contributions from each segment. For a circular membrane, the membrane displacement when there is a force over an annular region concentric with the membrane is given by

$$w_i(r) = \frac{F_i}{8D\pi}\left\{\frac{(r_m^2 + b_i^2)(r_m^2 - r^2)}{2r_m^2} + \left(b_i^2 + r^2\right)\ln\left(\frac{r}{r_m}\right)\right\}; r > b_i \tag{5}$$

and

$$w_i(r) = \frac{F_i}{8D\pi}\left\{\frac{(r_m^2 + b_i^2)(r_m^2 - r^2)}{2r_m^2} + \left(b_i^2 + r^2\right)\ln\left(\frac{r_m}{b_i}\right)\right\}; r \le b_i$$

where $w_i(r)$ shows the displacement due to the i^{th} capacitor; b_i and F_i are the radius of the i^{th} segment and the force over this segment, respectively. D is the flexural rigidity. The total membrane displacement is given by

$$w(r) = \sum_{i=1}^{N} w_i(r) \tag{6}$$

Since electrostatic forces change with membrane displacement, the steps shown above should be iterated until a convergence is obtained. The displacement at the center can be monitored to decide whether or not the solution is converged since the maximum displacement occurs at the membrane center.

The above approach was tested on an example of cMUT geometry shown in Fig. 2. Membrane displacement was calculated using finite element modeling by ANSYS and the proposed method. A total of 150 V DC voltage was applied to the top electrode. In addition to the electrostatic forces, atmospheric pressure was also taken into account. Fig. 3 compares the result, which shows a good agreement between the two methods.

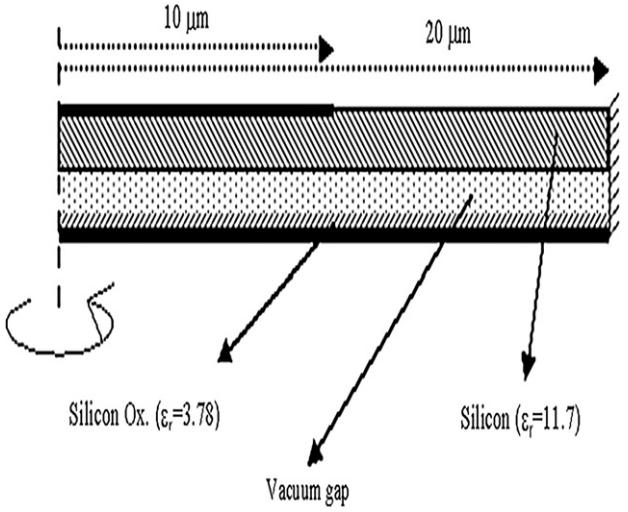

Fig. 2 CMUT geometry. Thick solid lines show the electrodes which are assumed to be inanity estimably thin [69]. cMUT = capacitive micromachined ultrasonic transducer.

The collapse voltage is found using a binary search algorithm. The membrane displacement is calculated using the method described above. If a voltage greater than the collapse voltage is applied to the membrane, the above method diverges instead of converging. Figs. 4 and 5 shows the center displacement for different bias voltages. By monitoring the second derivative of the center displacement with respect to iteration number, it can be determined whether the applied voltage is more or less than the collapse voltage.

Fabrication processes

We can categorize cMUT processes according to the highest temperature achieved throughout the entire process,

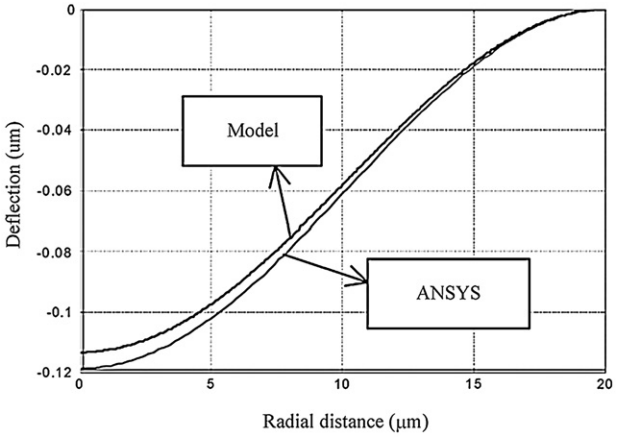

Fig. 3 Membrane deflection, calculated at a bias voltage of 150 V. There is also atmospheric pressure applied on the membrane [69].

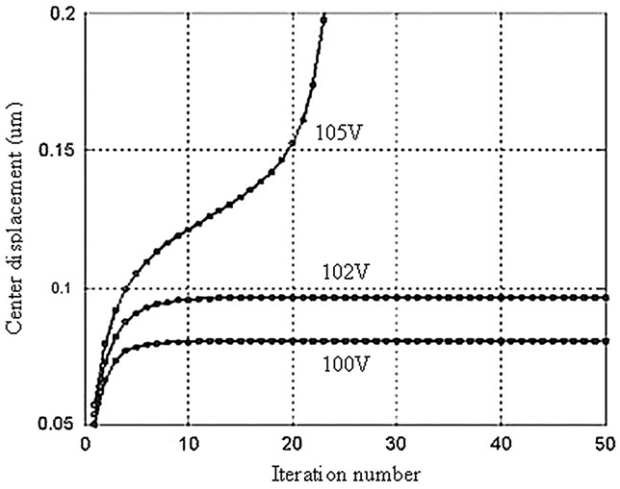

Fig. 4 Center displacement for different bias voltages as a function of iteration number [69].

because the highest temperature in the process has significant implications on the kind of electronic integration that follows. If the cMUTs are built on the same silicon substrate as the complementary metal-oxide-semiconductor (CMOS) electronic circuitry, then the highest temperature cannot exceed 400°C. Such processes are called low-temperature processes and are often referred to as CMOS compatible. All other types are simply called high-temperature processes. The wafer-bonding method, using fusion bonding, is clearly a high-temperature process, and is not compatible for post-processing on CMOS chips, although there are bonding processes that are compatible. The sacrificial release process can be high temperature or low temperature, depending on the type of deposition equipment used. The following sections will describe the high temperature sacrificial release process that uses the low-pressure chemical vapor deposition (LPCVD) technique for sacrificial layer and membrane depositions.

The membrane material is silicon nitride (Si3N4); the sacrificial layer material is polysilicon, which is selectively removed with potassium hydroxide (KOH) solution. Possible variations of the process (including the low-temperature process) are discussed and compared for performance, yield, and cost outcome [13].

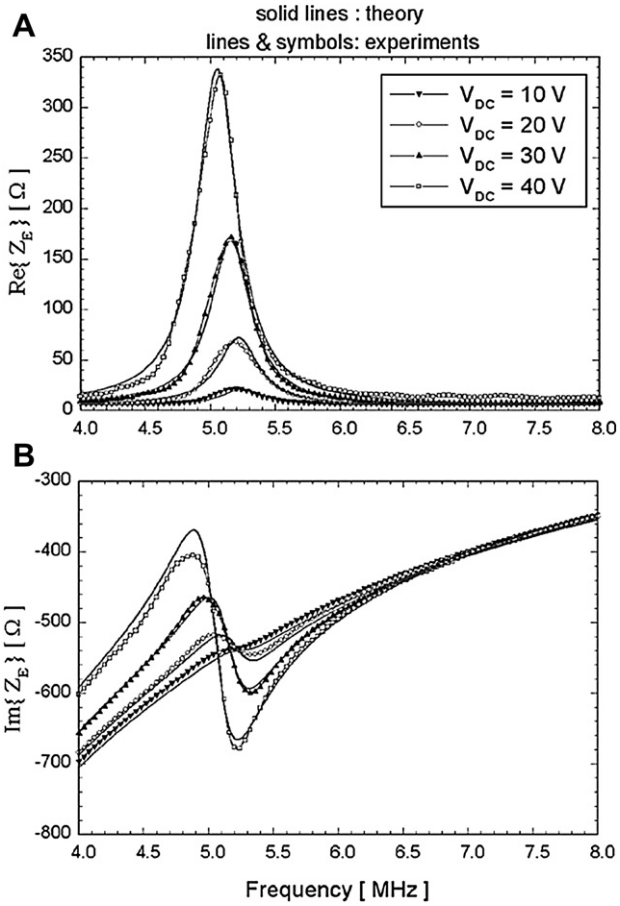

Fig. 5 Theoretical and experimental of (A) real part; and (B) imaginary part of the input electrical impedance of a cMUT [68]. cMUT = capacitive micromachined ultrasonic transducer.

Capacitive foil transducers

One approach to manufacturing cMUT followed precedent works regarding capacitive devices made of a thin plastic layer coated by a conductive film and tightened over a contoured metal back plate [14,15]. Such a membrane, being supported only at the high points (rail) of the back plate, acts as a series of small membranes (Fig. 6). The resonance frequencies of these small membranes depend on the distances between rails, and also on the mechanical tension of the plastic layer, together with the stiffness of air trapped in the small gaps between the membrane and the back plate. Hence, the control of the back plate's surface structure and of the mechanical properties of the thin membrane enables the control of the transducer's operation [16]. Silicon micromachining techniques have then been used to fabricate silicon back plates with the required accuracy [17,18]. In particular, bulk micromachining techniques have been employed to manufacture back plate structures with well-defined geometries. In fact, bulk micromachining has been the first technology to be used for the fabrication of microelectromechanical systems (MEMS). The micromechanical structures are manufactured in a silicon wafer by selectively removing parts of the wafer material, using orientation-dependent etching of single crystal silicon substrate. The bulk microfabrication process for the ultrasonic transducer back plate starts with the

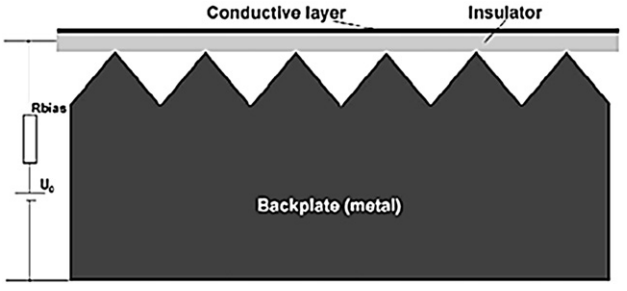

Fig. 6 The basic element of an electrostatic transducer [68].

deposition and patterning of a silicon nitride or a silicon dioxide layer as a mask, then (100)-oriented silicon wafers are etched in KOH aqueous solution, obtaining pits with triangular or trapezoidal cross-section, and with depth depending on the mask-opening dimension (Fig. 7). The so-micro machined silicon back plate is coated by a metallic layer and, subsequently, a polymer film with a thickness ranging from 2–13 μm, metalized on one side, is stretched over it and kept in tension by a metallic frame. Thanks to the small dimension of the micro membranes, suspended by the rails, the working frequency of these transducers can reach 1 or 2 MHz in air [17,19]. The membrane is forced to stay in contact with the rails due to the electrostatic pressure caused by the polarization voltage, and this constraint prevents down displacement of the membrane towards the substrate. But, as soon as the frequency increases, upward displacements are allowed. Due to this degree of freedom, and to the mutual mechanical coupling of the micro-membranes, regions in phase and out of phase appear on the surface of the membrane, destroying the coherence of the acoustic radiation [17], and limiting the range of frequency these transducers can operate.

Surface-micromachined capacitive ultrasonic transducers

Wafer bonding, considered as a bulk process, is widely used in micromachining, and older than surface micromachining techniques. There are three basic wafer-bonding techniques: anodic bonding, fusion bonding, and adhesive bonding. Among these techniques, silicon fusion bonding has earned a stable position in today's technology, and is now used for various applications: bond-and-etch back silicon-on-insulator (SOI) wafers, SMART-CUT SOI wafers, power devices, and many silicon microstructures, such as pressure sensors and accelerometers. Silicon fusion bonding is a direct bond between two silicon surfaces. It takes place at high temperatures, forming strong covalent bonds between the silicon wafers.

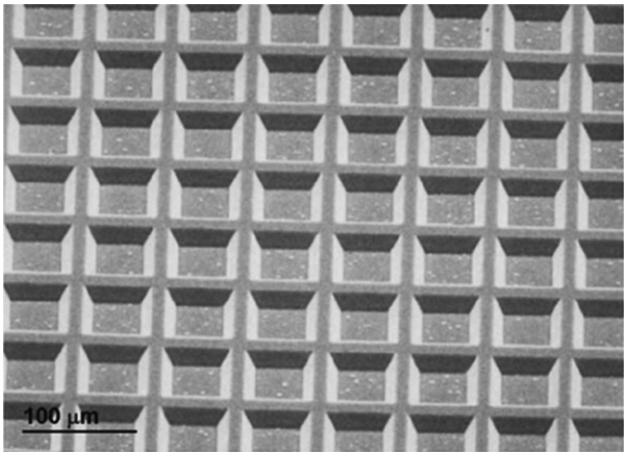

Fig. 7 Scanning Electron Microscopy (SEM) of a portion of a CMUT silicon back plate fabricated by anisotropic etching of silicon in KOH aqueous solution [68]. cMUT = capacitive micromachined ultrasonic transducer; KOH = potassium hydroxide.

Most of these techniques are based on surface micromachining techniques [2,20], others are modified BiCMOS processes [21], and others combine bulk and surface micromachining for the realization of the membranes and of the back plate [22].

In a surface-micromachining process, the micromechanical structures are fabricated by deposition on the silicon wafer of thin structural layers over thin sacrificial layers that can be selectively removed. Thin film deposition techniques, able to control the film's mechanical properties, such as internal stress or stress gradients, and dry and wet etchings that remove sacrificial layers without damaging the structural ones, are essential for surface micromachining as discussed below in this section.

The micromachining processes developed for the fabrication of cMUTs can be classified according to the maximum temperature used, which limits the degree of compatibility with IC processing and hence the possibility of integration of transducers and electronics on the same wafer.

The first process for the fabrication of cMUTs, based on surface micromachining techniques, was developed at Stanford University in Palo Alto, CA, USA [2]. The transducer is fabricated on a highly doped silicon wafer that acts as the fixed electrode. The membrane's structural material is silicon nitride deposited by LPCVD over a sacrificial layer of thermal oxide. Both the silicon nitride layer and the backside of the silicon wafer are coated with evaporated gold. Then a pattern of 3-μm diameter holes on a bidimensional grid with 100-μm period is transferred by lithography and etching through the gold and the silicon nitride layer to reach the sacrificial oxide. Then the membranes are released by wet etching of oxide in pure hydrofluoridric acid. The membranes' diameter is controlled by timed etch. The major manufacturing issue of this process consists in the membranes' release. The risk of fracture of the thin membranes and their sticking to the substrate can be avoided by properly choosing layer thicknesses, thin films' stresses, and membranes' dimensions. During drying after the sacrificial etching, capillary forces, proportional to the membrane area, which can be balanced by internal stress in the membrane, attract the membrane toward the substrate [23]. A thin membrane separated by a narrow gap from the back plate is the basic feature of the cMUT, but a membrane that is too thin easily collapses onto the substrate, and a thin gap limits the membrane's displacement during operation. A large value of the internal stress in silicon nitride film increases the resistance to collapse, but it can cause the membrane to break, resulting in yield loss; furthermore, it affects the resonance vibration frequency of the membrane in air. As a consequence, the cMUT presented by Haller and Khuri-Yakub [2] had a 0.75-μm thick membrane suspended on a 1-μm thick gap. The silicon nitride layer was deposited by LPCVD using a mixture of ammonia and dichlorosilane at 800°C in order to tune the residual stress of the membrane at a value of 280 MPa.

Another issue of the process is the timed etch of the sacrificial layer. The etching rate decreases with time as the etchant and the etch products must diffuse longer through the small holes in the structural layer. The membrane's diameter depends on the etching duration and only circular membranes can be obtained, as the etch

proceeds isotropically. In addition, the etching selectivity of the sacrificial layer against the structural one is not 100%, causing a modification of the membranes' thickness near the etchant holes.

Finally, a further important concern is that the cavities below the membranes can be contaminated by humidity or entered by particulates through the etchant holes. Ladabaum and colleagues [24] addressed this last issue by using electron beam lithography to define a pattern of submicron etchant holes, and then transferring it to the silicon nitride structural layer. These narrow holes are efficiently sealed by a deposition of a thin layer of LPCVD silicon nitride. In fact, the material is conformally deposited on the edges of the hole, which is closed before any material penetrates the cavity under the membrane. As the deposition is made at low pressure, the cavity results in being vacuum-sealed. Besides, using small via size, the membrane's geometry can be defined by the pattern of the holes and problems related to long-time etching will be overcome [25].

A better control over the critical process steps necessary for manufacturing the transducer in a robust manner has been presented by Jin and colleagues [24]. LPCVD silicon nitride is still used as a structural layer, but silicon oxide has been replaced by amorphous silicon as a sacrificial layer because of its good etching selectivity against the membrane layer. Furthermore, prepatterning of the sacrificial layer by lithographic and etching steps before the structural layer deposition, allows better control of the cell size under the membrane, which no longer depends on timed oxide etching. In Fig. 8 the major steps of the process flow, including prepatterning for the fabrication of cMUT is illustrated.

Jin and colleagues [26] manufactured the fixed electrode at the n-type silicon wafer surface by heavily doping with phosphorus at 1000°C. As the sacrificial material is amorphous silicon, an etch stop is necessary between the silicon wafer and the sacrificial layer, thus a thin LPCVD silicon nitride film is deposited at 800°C. Amorphous silicon is then deposited at 560°C and patterned into hexagonal

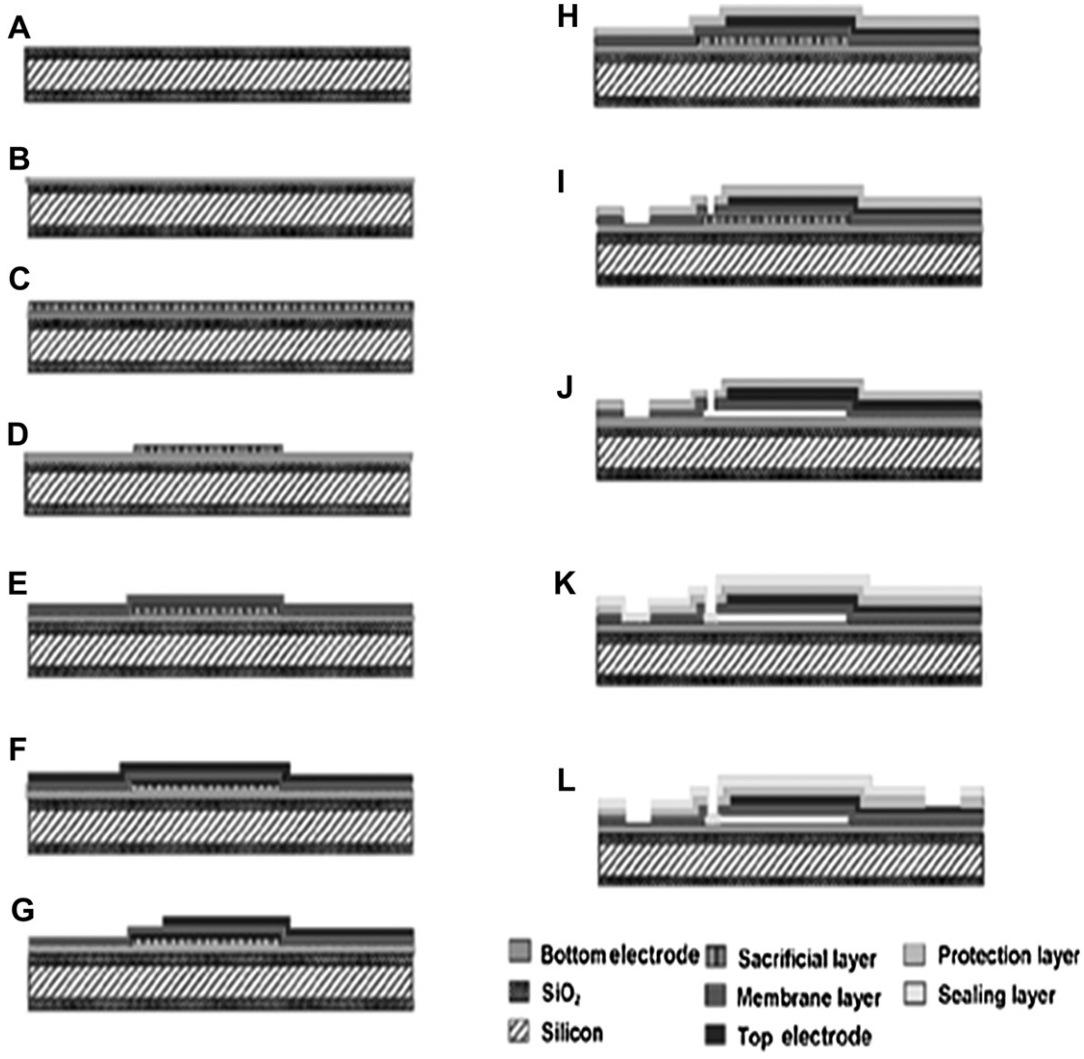

Fig. 8 Surface micromachining process flow for the fabrication of CMUTs: (A) thermal oxidation; (B) bottom electrode fabrication; (C, D) deposition and pre patterning of the sacrificial layer; (E) deposition of the membrane structural layer; (F, G) top electrode fabrication; (H) passivation; (I) opening of the via; (J) removal of the sacrificial layer; (K) hermetical sealing; (L) etching for contact pads. cMUT = capacitive micromachined ultrasonic transducer.

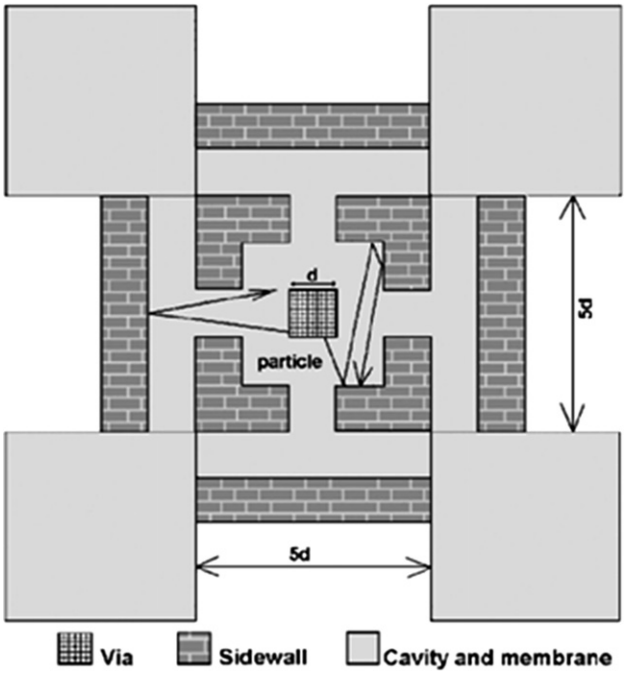

Fig. 9 Buffered lateral sealing [68].

islands that will form the transducer's active regions. The thin membrane is made of LPCVD SiN deposited at 800°C with low tensile stress. Etching in aqueous KOH at 75°C removes the sacrificial amorphous silicon through the 2-μm diameter etchant holes opened along the island perimeter. As the membrane is released, the holes are vacuum-sealed by a low thermal oxide (LTO) deposition. LTO has been chosen for its high sticking coefficient, as it closes the via without largely penetrating into the cavity under the membrane.

A configuration of via and etch channels away from the cavities (Fig. 9) was developed to limit the penetration of sealing material inside the cavity and to preserve the original thickness of the cavity and membrane [25]. The etch hole is placed in the area among four adjacent membranes; beneath the hole is a region surrounded by vertical sidewalls with apertures towards etch channels that connect the four sacrificial islands. The material deposited to seal the via penetrates in the region underneath the via and it is almost kept there by the vertical sidewalls, not entering the cavity. On the other hand, this etch-hole configuration utilizes a large area among adjacent membranes, limiting the number of active cells per unit area that defines the transducer's filling factor.

Another high-temperature process for the fabrication of cMUT, which overcomes the steps of opening vias for sacrificial etching and subsequent sealing, is based on a wafer-bonding technique and on the use of an SOI wafer [22]. The membrane is made of the SOI silicon device layer, whereas the cavity is fabricated on a low-resistivity silicon wafer. They are then bonded together to form the cMUT (Fig. 10). Cavities less than 2-μm in depth are manufactured in a silicon dioxide layer thermally grown on the silicon wafer; otherwise, to obtain deeper gaps, they are etched in silicon, using the oxide film as a mask and aqueous KOH solution for etching. The SOI wafer and the back plate wafer are bonded in a vacuum and then annealed at 1100°C to ensure effective bonding. Then the handle wafer and the buried oxide of SOI are removed in

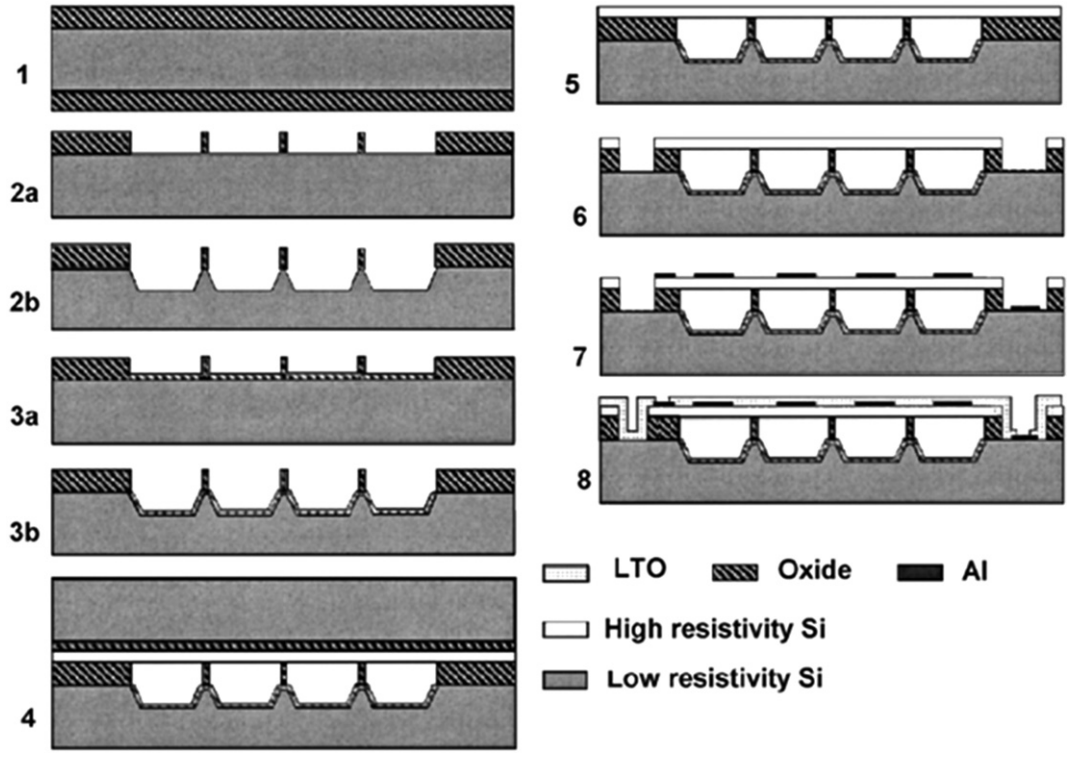

Fig. 10 The steps to fabricate wafer-bonded CMUTs [68]. cMUT = capacitive micromachined ultrasonic transducer.

KOH and hydrofluoric acid (HF), respectively, leaving the membrane suspended over the back plate by thin oxide supports. The membrane comprises single-crystal silicon, which is stress free, has low defects, is of uniform thickness, and fabricated in a controlled and repeatable way by the SOI wafer industry. It is a planar film with no holes, suspended over vacuum-sealed cavities, with the shape and size precisely controlled by means of a lithographic and etching step, and not modified by any sealing deposition step. Membranes with a diameter ranging from 12—750 μm, and a thickness of between 0.34—4.5 μm have been fabricated. For the cMUT, the active silicon layer is metalized and patterned to make the top electrode, and coated by a LTO layer for passivation.

The processes described above do not allow the integration of electronics and transducers on the same cMUT wafer, because the high temperature steps in the cMUT fabrication are not compatible with IC processing. Then a two-chip approach can be used, building the transducer on one chip, the control electronics on another, and then wire bonding them together.

However, for high-density 2-D cMUT arrays, made of thousands of elements, addressing each individual element by wire bonding becomes an issue. In addition, the parasitic capacitance of the interconnection between the cMUT element and its electronics limits the transducer's performance. A solution is based on through-wafer interconnect technology [4,27]. Wire bonding is replaced by through-chip via that bring the interconnections from the front-side of the cMUT wafer to the back side of the wafer, and then the cMUT wafer can be flip-chip bonded to the wafer containing the signal processing electronics. The high aspect ratio via are manufactured by deep reactive ion etching: 20-μm diameter channels are etched through a 400-mm-thick silicon wafer (Fig. 11A). To further reduce the parasitic capacitance, the capacitors formed by the bulk silicon substrate and the polysilicon pads for top and bottom electrodes, and the via through the wafer must be taken into account. They are minimized implementing reverse-biased pn junctions between the pads and the wafer, and a reverse-biased metal-insulator-semiconductor junction inside the via (Fig. 11B). When the junctions are reverse biased, the silicon wafer is electron depleted, resulting in a low parasitic capacitance [4].

CMOS-compatible fabrication processes for cMUTs

Alternative fabrication processes for cMUTs are based on low-temperature thin film deposition techniques or on modified CMOS processes, resulting in compatible integration with the transducer and signal conditioning electronics on the same wafer. In a modified CMOS process [28], the membrane is made of polysilicon over the field oxide, which is removed as the sacrificial layer to release the membrane. This is the only additional step introduced in the standard BiCMOS process flow for cMUT manufacturing. Membranes with diameter ranging from 20—100 μm and thickness between 0.5 and 4 μm have been fabricated. The transducers can be monolithically integrated with electronics on one chip, hence reducing parasitic capacitance and improving signal-to-noise ratio (Fig. 12).

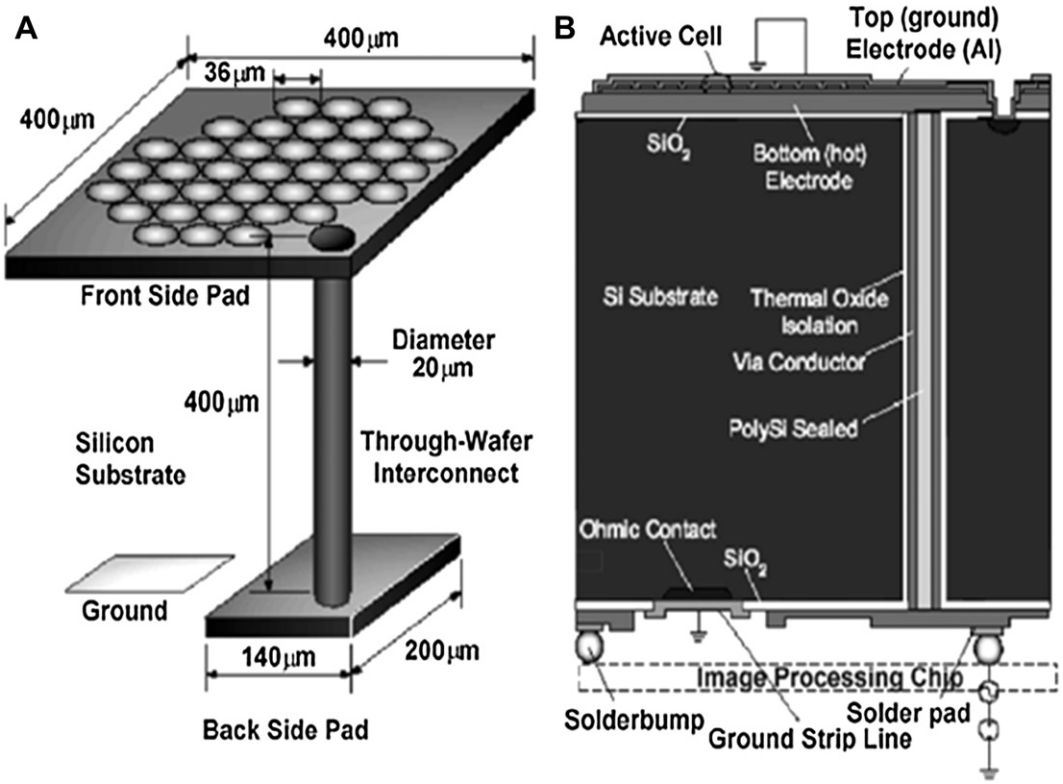

Fig. 11 (A) a metal-insulator semiconductor junction (MIS) through wafer via schematics; (B) a metal-insulator semiconductor junction (MIS) through the wafer cross section [68].

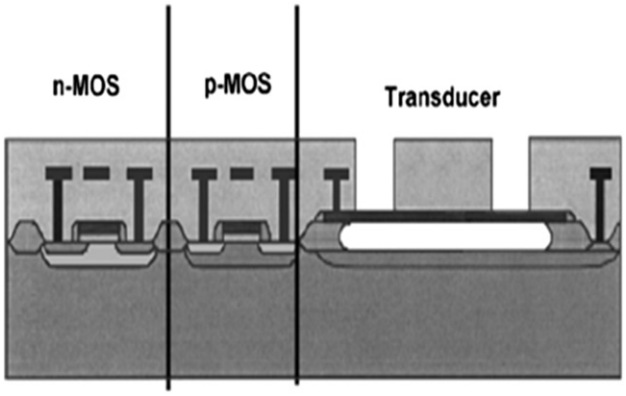

Fig. 12 Structure of the integrated ultrasonic transducer cell and Complementary metal-oxide-Semiconductor (CMOS) transistors [68].

In the proposed low-temperature processes for cMUTs [20,28,29], the structural material for the membrane's fabrication is silicon nitride, deposited by plasma enhanced chemical vapor deposition (PECVD).

The use of PECVD allows for the deposit of silicon nitride structural layers at low temperature ($\leq$400°C), with such characteristics as mechanical stress, density, resistivity, and etch rate controlled by the deposition parameters. In addition, the low temperature permits the use of a wide range of materials for sacrificial layers and for metallization. Polyimide layers, spin-coated on silicon substrates, have been used as sacrificial material underneath the PECVD silicon nitride membranes, because cured polyimide is not modified at 400°C. It can be removed by wet etching, with perfect selectivity with respect to structural layers [28], and also by dry etching in plasma of Tetrafluoromethane (CF_4) and O_2 [20]; this allows station problems to be overcome and the fabrication of large membranes, provided micrometric etchant holes are placed on the membrane's area to give sufficient access to plasma for sacrificial removal. On the other hand, such large holes on the membrane are difficult to seal without affecting the cavity underneath.

As already discussed, the mechanical properties of the membrane structural layer affect the performance of a cMUT; PECVD silicon nitride is characterized by poorer properties than LPCVD, i.e., lower density, lower Young's modulus, and higher etch rate in HF and KOH [30], but it can be optimized as a structural layer for micromachined free-standing membranes, and its internal stress can be tuned varying the deposition parameters, as Radio Frequency (RF) power [20] or relative flow rates of reactant gases [31]. PECVD silicon nitride is deposited using saline, ammonia, nitrogen, and helium at temperatures lower than 400°C. By increasing the ammonia to a saline flow-rate ratio, the internal stress changes from compressive to tensile as it can be monitored by the change in the membrane's deformation. In fact, as the membranes are suspended over the cavities by elastic supports, the residual stress in the film pushes the supports, and the membrane bends downward or upward, depending on whether the stress is tensile or compressive; the membrane stands flat if the structural layer is stress free (Fig. 13).

The cavities are sealed by a PECVD silicon nitride deposition that fills the vias placed on small regions protruding from the membrane's perimeter in Fig. 14A and does not penetrate the cavity. The top electrode is fabricated by sputtering deposition and patterning of a metal layer at the top of the membrane, and it is finally protected by a thin PECVD silicon nitride layer. The contact windows on pads are opened by dry etching. Fig. 14B shows a single element CMUT, made of 1512 electrostatic cells, covering an area of 3 mm^2.

To fabricate the multielement cMUT array, the process is the same of that of single element transducers, except for the photolithographic masks, as shown in Fig. 15, where a portion of a cMUT array is shown. The array comprises rectangular elements (230-μm wide, 12-mm long, with a 15-μm separation between the adjacent elements), with the sealed active cells aligned over the rectangular bottom electrodes, and the contact pads, for connecting each element by wire bonding to driving circuitry [68].

Applications

The applications of cMUTs can be divided into two main categories, (1) air applications, and (2) immersion

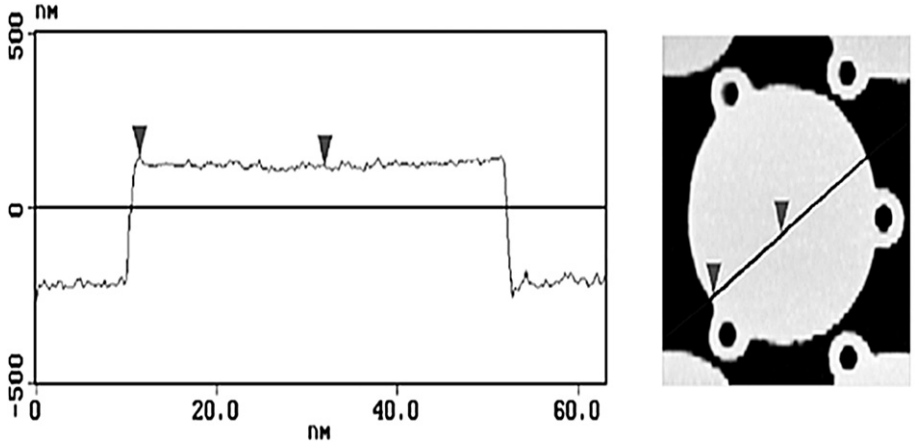

Fig. 13 Atomic force cross-section profile and topography of a CMUT membrane after release. The membrane's diameter is 40 μm and the diameter of the vias is 40 μm [68]. cMUT = capacitive micromachined ultrasonic transducer.

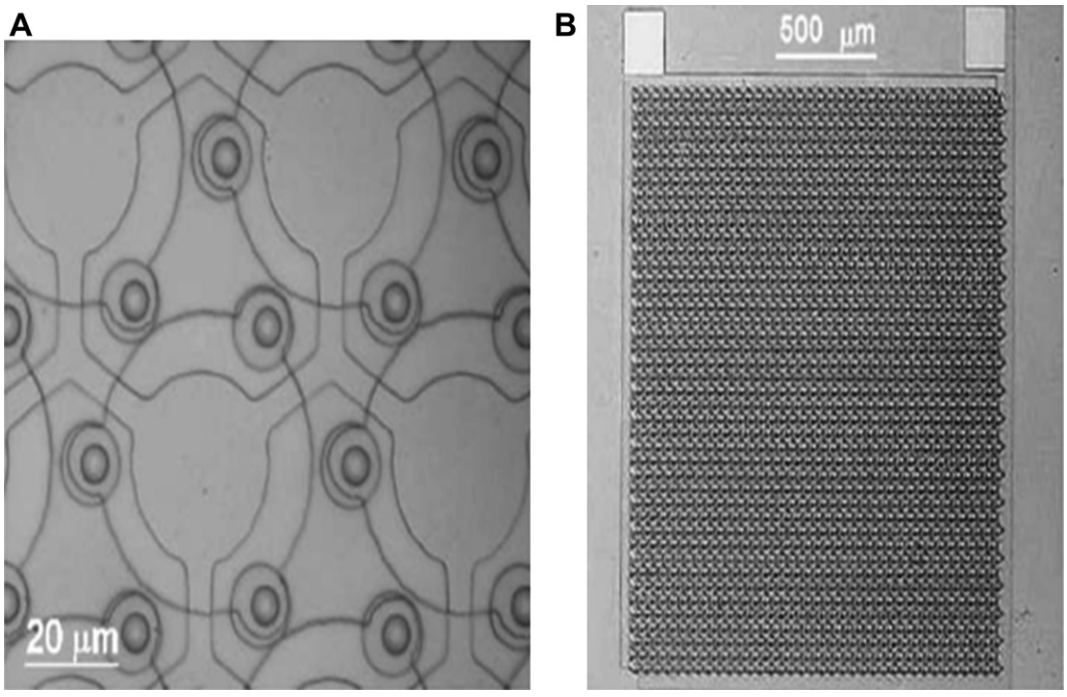

Fig. 14 (A) Photograph of a portion of a fabricated CMUT, showing a top view of some membranes with the sealed vias and the top electrode; (B) photograph of a single-element 3-mm^2 CMUT, with the two contact pads for connection of the fixed electrode at the bottom of the cells and the free electrode at the top of the membrane [68]. cMUT = capacitive micromachined ultrasonic transducer.

applications. Air applications refer to cases where the membranes are loaded with air or a gas. Similarly, immersion applications refer to cases where the loading medium is a fluid. The following subsections will discuss these applications and show device examples, while highlighting the advantages and disadvantages of cMUTs [69].

Immersion applications

Immersion applications refer to cases in which the transducer is loaded with a fluid or a mechanically equivalent solid. For example, medical imaging, in which the subject is mostly the human body, is considered an immersion

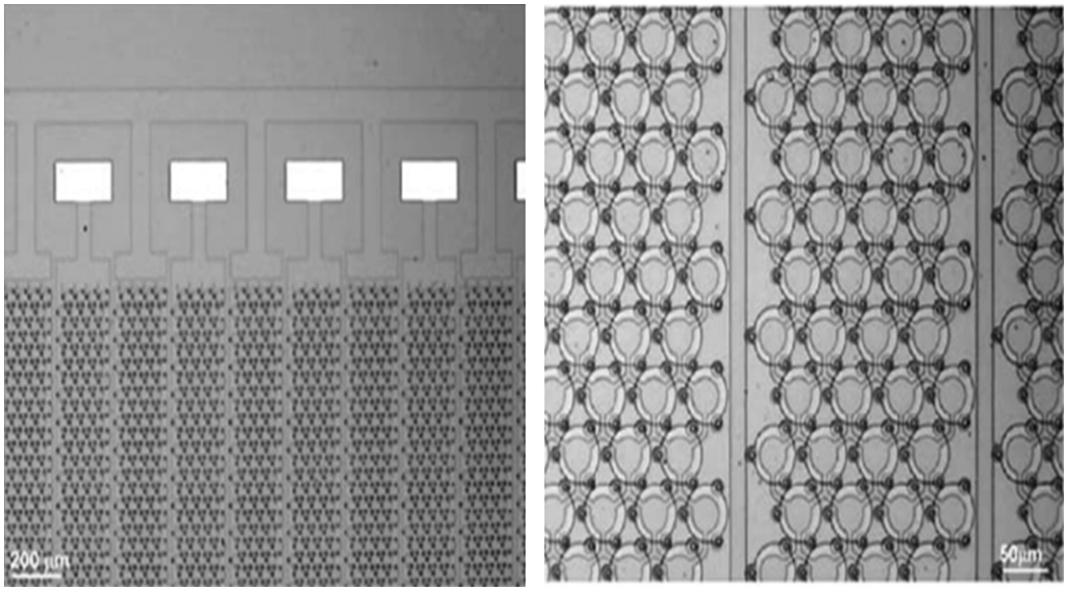

Fig. 15 Photograph of a portion of a CMUT array, made of rectangular elements (pitch, 250 μm; elevation, 12 mm), showing the sealed active cells aligned over the rectangular bottom electrodes; the contact pads that are contacted by wire bonding to drive each element [68]. cMUT = capacitive micromachined ultrasonic transducer.

application. All of the above-mentioned air applications ranging, flow metering, and nondestructive testing (NDT) have an immersion version. Sonar, for example, is underwater ranging. Flow metering, when done in fluid pipes, is an immersion application. In some NDT applications, the target(s), together with the ultrasonic transducer(s), can be immersed in a neutral fluid, where ultrasound is coupled to the target through the fluid. Because cMUTs are mostly fabricated with sealed cavities, air cMUT transducers can also operate in immersion. However, the size of the transducer and the cavity height must be designed properly for optimum operation in fluids. Fluids have acoustical impedance three to four orders of magnitude higher than air. Therefore, fluid loading over damps the normally resonant membranes of cMUTs, which results in exceptionally wide bandwidth operation, which is one of the most important benefits of using cMUTs in immersion. Besides, the electrical match is not as great as it is in air applications, and is typically 10 dB or larger. In sonar applications, there are traditionally two main issues: bandwidth and the size of low-frequency transducers. When space is limited, as in unmanned underwater vehicles (UUV), managing these issues becomes a challenge. Because cMUTs are inherently wide-band transducers in immersion applications, they can help solve such challenges. Consider the device example in the insert of Fig. 16. The device is a single element sonar transmitter, 75-mm in diameter, comprising 650-μm wide and 4.2-μm thick square membranes. The frequency response was measured by a pulse-echo experiment where the single tone burst pulse was reflected from a plane reflector at 10 cm. Both the transmitter and receiver of the cMUT transducer was biased to 100 Vin (bias DC voltage power supply). The received echo signal was converted to a frequency response by fast Fourier transformation (FFT), which was later corrected for diffraction. This single element sonar transmitter has a frequency range extending from 10—180 kHz, which would usually be covered with two to three piezoelectric transducers. The device was fabricated using the wafer-bonding method [22] on a 0.5-mm-thick silicon substrate. By contrast to the thickness of the thickness-mode piezoelectric transducers at these frequencies, cMUTs are low-profile devices. That is, several piezoelectric transmitters may be replaced by a single cMUT sonar transmitter.

Immersion flow metering and NDT applications also benefit from wide-band cMUT transducers. Wide-band, high-frequency (a few MHz) transducers can be employed to reduce noise in flow-metering applications and to increase the detection resolution in NDT applications. Fig. 17A shows the pulse-echo experiment setup, and Fig. 17B shows the frequency response of another device example that is 7 mm × 7 mm in size, and has a 96-μm diameter and 0.5-μm-thick circular membranes. The frequency response was obtained by a similar pulse-echo experiment as explained above. The transducer was excited by a 20 V, 200 ns pulse on top of 100 V bias. As the plot (Fig. 17B) clearly depicts, the device has wide frequency bandwidth extending from 0.5—2.5 MHz, without any matching layer or matching network.

Although the above-mentioned applications benefit from the superior properties of cMUTs, there hasn't been much interest in those applications. The biggest interest in

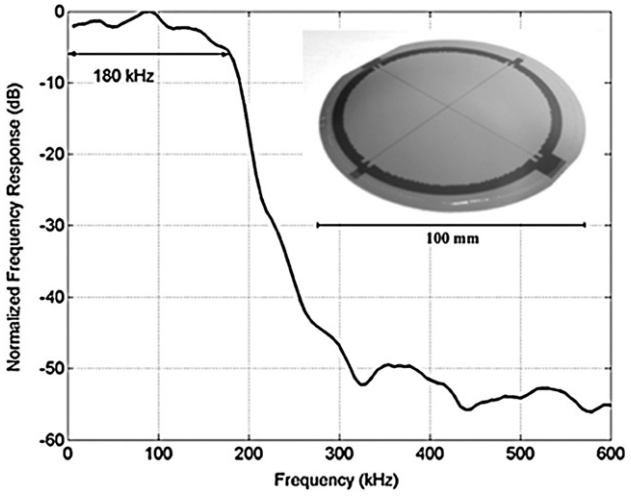

Fig. 16 Frequency spectrum of a sonar transmitter, 7.5-cm in diameter, made of 650-μm-wide square membranes. The spectrum is obtained from the pulse-echo response, where the transmitted signal was reflected from a plane reflector 10 cm away. The response, which covers the frequency range from 10—180 kHz, is corrected for diffraction [69].

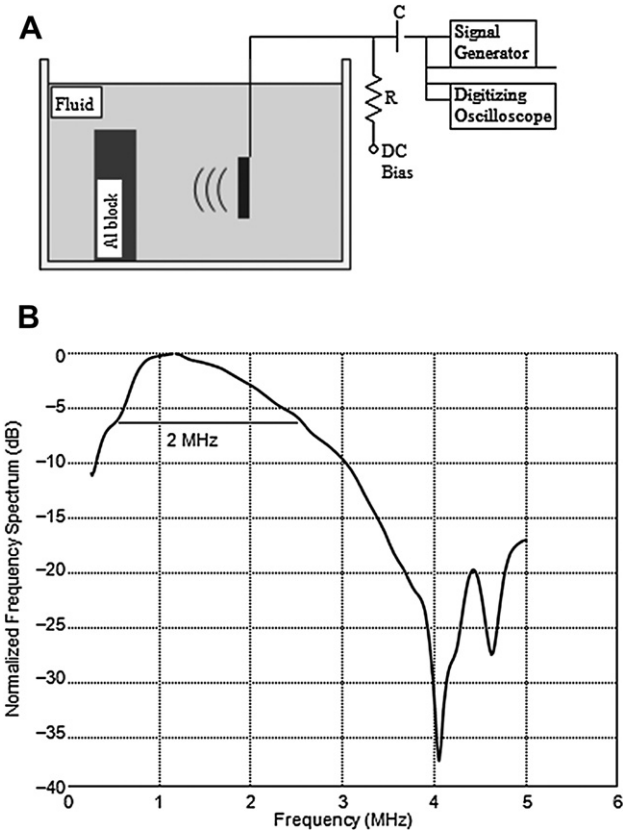

Fig. 17 (A) Pulse-echo experiment setup to obtain frequency response in immersion; (B) immersion frequency response of a 7 mm × 7 mm device, which extends from 0.5—2.5 MHz. The response is corrected both for diffraction and attenuation in the fluid [69].

immersion cMUTs has been in underwater and medical imaging applications using one-dimensional and 2-D arrays. There are four reasons for this interest: exceptional immersion bandwidth of cMUTs, frequency range that is covered by the technology (10 kHz—60 MHz), scalability of the micromachining technology, and low manufacturing cost. In ultrasound imaging, at a given frequency, the depth resolution is determined solely by the length of the ultrasonic pulses generated by the transducer array elements. In other words, to be able to resolve between two very close reflectors in the imaging plane, the echo signals coming from the reflectors must be separate in time, which is possible only with short ultrasound pulses. Because the pulse length is inversely proportional to the frequency bandwidth, using wide-band cMUT arrays increases the depth resolution. Fig. 18 shows a picture of a one-dimensional array designed for underwater imaging. The top part of the figure shows the 100-mm wafer on which the arrays were fabricated. Each wafer contains eight arrays, each with 86 elements. The lower part of the figure shows

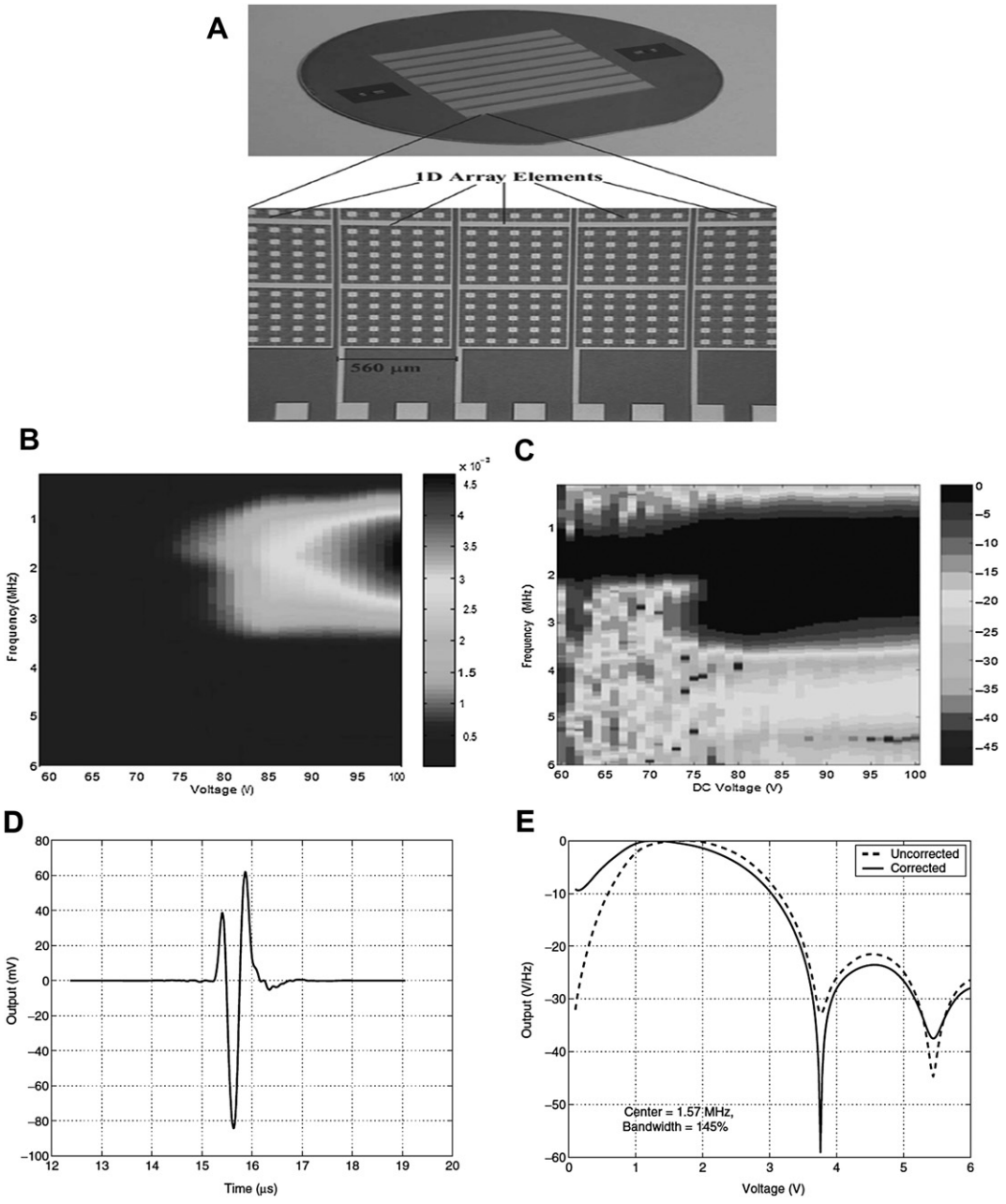

Fig. 18 (A) Picture of a one-dimensional array designed for underwater imaging. Four elements, connected together for the pulse-echo experiment, were excited with a single-cycle tone burst at 1.85 MHz. The bias voltage was increased to 100 V with 1-V increments, and the echo signals were collected with a computer at each voltage increment; (B) shows the FFT of the received signals on a color plot; (C) is the normalized version of the FFT map for each voltage increment; (D) shows a sample echo signal measured at 100 V bias; (E) shows its uncorrected (black line) and corrected (red line) normalized FFT spectrum [69]. FFT = fast Fourier transformation.

the array elements in detail. Each element is 560-μm wide and comprises 200 square membranes, which are 96-μm in size. Four elements were connected together for the pulse-echo experiments, and excited with a single cycle, 10 V peak tone burst at 1.85 MHz. The reflector was located 1.1-cm away from the cMUT array, and the echo signal from the reflector was collected using the same elements. The bias voltage was increased to 100 V with 1 V increments, and the echo signals were collected at each voltage increment using a computer. Fig. 18B and C show the FFT of the echo signals (raw and normalized, respectively) on a color plot. As the time domain response clearly shows, the cMUT arrays have wide frequency bandwidth, from 0.4—2.7 MHz. Similarly, both lateral and depth resolutions are inversely proportional to the imaging frequency. That is, the size of the smallest pattern or structure that can be resolved decreases as the frequency of operation increases. However, the attenuation coefficient of sound in water is proportional to the square of the frequency, which means that the attenuation will increase and the imaging range will decrease dramatically for high-frequency ultrasound.

The shortcoming of cMUTs in immersion applications has been the output pressure capability, which is lower than the competing piezoelectric transducers. Increasing the fill factor and average displacement by using rectangular membranes [37] improves the output pressure capability as well as the receive sensitivity. There is also a new regime of operation [38—42,52—54] under investigation, in which the cMUT membranes are operated in collapse mode. In this mode, cMUT membranes are collapsed intentionally so that the center of the membrane is pinned to the substrate, and the ring around the center is vibrating. Because very high electric fields are sustained around the collapsed region, it is possible to generate high-output pressures as well. The close proximity between the membrane and the bottom electrode around the collapsed region also improves the receive sensitivity and matching to the electronics. In medical imaging, there is growing interest in miniature, volumetric imaging devices, mainly for in vivo applications [43,44], such as intravascular imaging, surgical guidance, etc. Because of the scalability of the micromachining process (like the scalability of the integrated circuit processes), manufacturing of miniature cMUT arrays is easy. The membranes and elements are defined by photolithographic techniques. Therefore, manufacturing an array of cMUTs is equivalent to manufacturing a single element cMUT. The only exception is when electrical through-wafer interconnects are involved, which adds a number of steps to the fabrication process. When integrated with electronics through wafer interconnects and flip-chip bonding, miniature cMUT arrays will be very powerful imaging tools *in vivo* applications.

Air applications

Air applications highlight two very distinct features of cMUTs: excellent match to air with very high coupling efficiency, and temperature tolerance. The latter is a feature of the materials that make up cMUTs. Usually, the substrate is silicon and the membrane material is either silicon or silicon nitride, both of which have very high melting points. The temperature limit is more likely to be determined by the metal layer used. The stress that develops at very high temperatures because of the difference in the thermal expansion coefficients of the layers can be taken into account during the design stage. The most attractive feature of cMUTs in air applications is its excellent match to air (or other gases), a consequence of the low mechanical impedance of thin membranes.

Consider a device example that is 7 mm × 7 mm in size, fabricated using the silicon nitride technology. The device is made of 7056 circular membranes, each of which has a diameter of 80 μm. The membranes are silicon nitride and 1-μm thick. The gap height is 0.8-μm before deflection due to atmospheric pressure. Fig. 19A shows the deflection curves of the membrane at various bias voltages ranging from 0—170 V. The deflection curves were obtained using a white light interferometer (Zygo-Veeco, Middlefield, USA). Notice that the membranes are deflected by a 0.25-μm at 0-V bias that is caused by the atmospheric pressure. The input impedance of this device was measured using a vector network analyzer (HP8751) and a power supply (SRS P310). Both pieces of equipment were controlled through a General Purpose Interface Bus (GPIB) interface and the input impedance data was collected with 1-V increments. Fig. 19B shows a sample input impedance data at 140-V bias. The imaginary part of the impedance crosses the x-axis twice. The first crossing is the short-circuit resonance where the membrane displacement is maximum, and the second crossing is the open-circuit resonance where the real part of the impedance makes a peak. Fig. 19C shows the short and open-circuit resonances as a function of the bias voltage from which the electromechanical coupling efficiency is calculated. As Fig. 19D reveals, it attains a value of 0.8 at a 180-V bias. The electrical input impedance data was used to calculate the insertion loss of the cMUT device. Fig. 20A is the plot of the insertion loss together with the center frequency as a function of the bias voltage. As the figure reveals, the cMUT device is matched to 50 Ω very well (without any matching layer or electrical matching network) for bias voltages above 80 V, and the center frequency is tunable between 1.25—2.75 MHz. Fig. 20B plots the 3-dB bandwidth of the insertion loss, which shows that close to collapse voltage, and the bandwidth of the cMUT device increases significantly (60% fractional bandwidth in air). This is a consequence of the spring softening effect, described in the modeling section, and comes without any matching effort. Fig. 20C is a plot that shows the effect of active area coverage, where the device with circular membranes is compared to a device made of 8016 hexagonal membranes. Because the hexagonal membranes were packed more densely in a hexagonal grid, the active area coverage was increased from 73%—86% for the device with circular membranes. This reflects a better match to 50 Ω at lower bias voltages, and a better match to lower source impedances. Fig. 20D compares the insertion loss for a 5-Ω system, showing that the device with higher active area coverage has a better match. Note that a 5Ω system can deliver 10 times more power than a 50-Ω system.

The dynamic range of this device, defined as the ratio of the output pressure per volt excitation to the minimum detectable pressure, was estimated to be 160d B/V. A low-

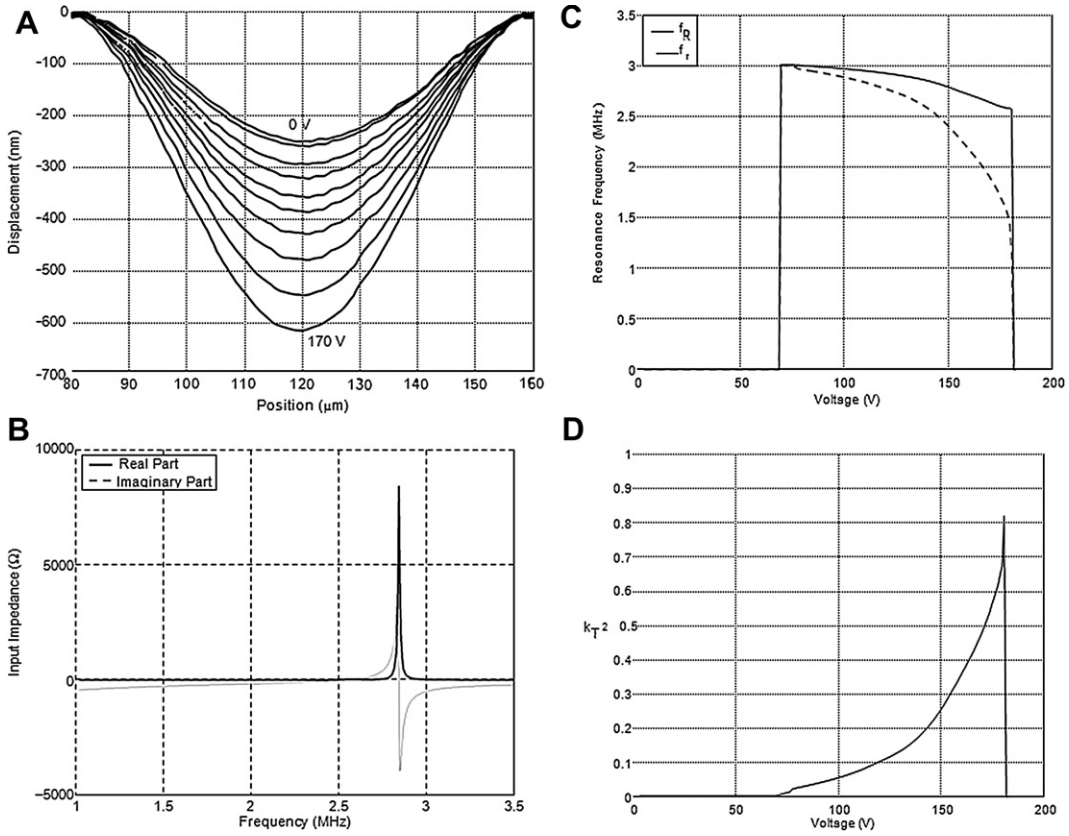

Fig. 19 A 7 mm × 7 mm cMUT device operating in air: (A) static deflection curves of the membrane at various bias voltages are measured using a white light interferometer from Veeco; (B) input impedance data in air is measured using HP8751 network analyzer (bias voltage is 140 V); (C) short-circuit (f_Y) and open-circuit (f_R) resonant frequencies are plotted as a function of bias voltage; (D) electromechanical coupling coefficient, as calculated from the short and open circuit resonant frequencies, is plotted as a function of bias voltage [69]. cMUT = capacitive micromachined ultrasonic transducer.

noise amplifier with an input impedance of 50 Ω and an input referred noise voltage of 1 nV/vHz was used in making this estimation. The dynamic range of a transducer is a measure of the total loss the system can tolerate and still receive a signal with a signal-to-noise ratio of one.

Thus, at 2 MHz, this device has a range of 24-cm in air, which increases to 1 m at 1 MHz. This also means the acoustic signal can go through solids despite the large impedance mismatch with air, and still be detected (for aluminum, the two-way acoustical mismatch loss is 80dB) with good Signal to noise ratio (SNR). Electrical and acoustical matching, high electromechanical coupling efficiency, and bandwidth are key features for air applications such as ultrasonic ranging [32,33], gas-flow metering [34], and NDT of fracture/crack in solids [6,35]. Ultrasonic ranging is measuring the distance of a target from the ultrasound source, and is done by a pulse-echo measurement, either with a single transducer or with a transmit/receive pair, and by measuring the time of flight. The distance to the target is calculated using the speed of sound in air. Ultrasonic ranging using piezoelectric transducers and conventional electrostatic transducers have been in use in many fields, such as auto-focus cameras, motion detectors, proximity sensors, and robotics. In addition to the high dynamic range (longer range detection), cMUTs offer three more significant advantages. First, because of the way they are built (sealed cavity), cMUTs have excellent tolerance to humidity, particles, and, with a proper choice of materials during the fabrication process, to most chemicals. The second advantage, which is also a consequence of the sealed cavity, is the ability to generate high-frequency ultrasound (a few MHz in air) with high efficiency. Although using high-frequency ultrasound decreases the range in air considerably, it increases the accuracy in localizing and tracking targets and enables detection of smaller targets. Finally, cMUTs can be fabricated in the form of arrays, which makes acoustic beam shaping and steering possible. Together with the relatively wide bandwidth of cMUTs in air (compared to piezoelectric transducers and conventional electrostatic transducers), using an array of transducers can increase the accuracy of locating objects in a multiobject environment. Gas-flow metering using ultrasound can be done in two ways, (1) with two transducers facing each other in the direction of the flow, or (2) with an array of transducers facing a reflector perpendicular to the direction of the flow (Fig. 21).

In the former, one of the transducers is used to transmit ultrasound parallel to the flow, and the other is used to detect the transmitted signal. The measurement is repeated by reversing the transmitter and receiver pair (or it can be done simultaneously). The flow speed is measured by

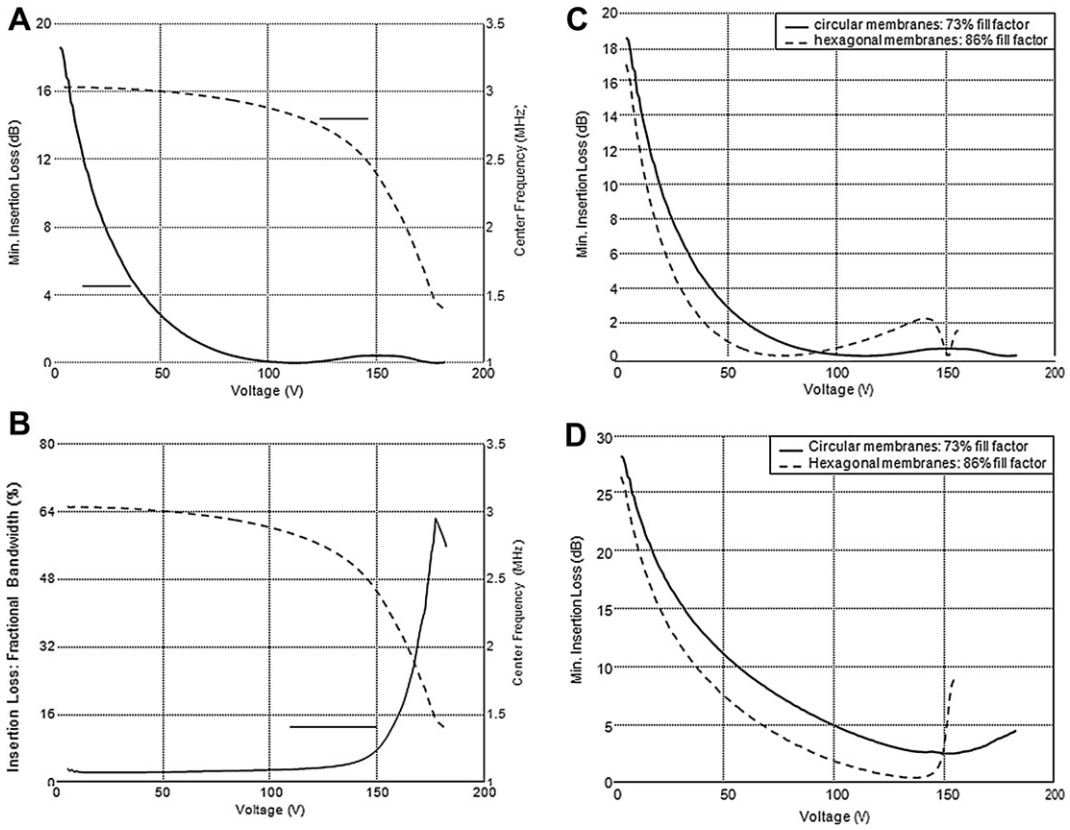

Fig. 20 A 7 mm × 7 mm cMUT device operating in air: (A) minimum insertion loss; (B) 3-dB bandwidth of the insertion loss, as calculated from the input impedance data of the device; (C) circular and hexagonal membranes are compared for a source impedance of 50; and (D) 5. The hexagonal membranes are tightly packed with active area coverage of 86%, whereas the circular membranes are packed on a square grid resulting in active area coverage of 73% [69]. cMUT = capacitive micromachined ultrasonic transducer.

measuring the difference in the time of flights. In the latter, one of the elements of the array is used as a transmitter and the relative amplitudes and phases received by the array elements determine the direction and magnitude of the flow.

The first method assumed that the temperature and the density of the gas are constant or measured by some other means. Because the speed of sound in a gas is a strong function of both temperature and density, the time of flight measurement will depend on all three components: flow rate, temperature, and density of the gas. In the second method, the flow rate is measured independent of the temperature and density, by measuring the direction of the transmitted ultrasound. In addition, the second method allows simultaneous measurement of temperature and density, using time of flight and electrical input impedance measurements [36]. The high efficiency and the relatively large bandwidth of cMUT transducers offer several advantages in flow metering as well. The ability to generate short ultrasound pulses (per large bandwidth) increases the SNR of the received signal and allows the use of chirp signals to improve SNR even further [34]. In low-pressure environments in which acoustical impedance of the medium is lower than air, the low mechanical impedance of cMUTs presents an even greater advantage.

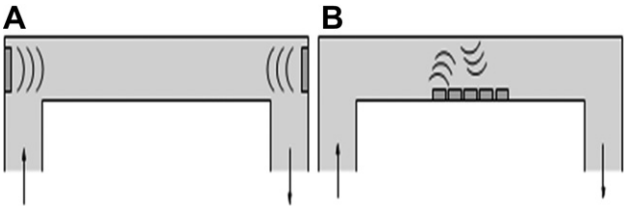

Fig. 21 Ultrasonic flow-metering methods: (A) parallel to the direction of flow; (B) perpendicular to the direction of flow [69].

Nondestructive testing (NDT) refers to the evaluation of solid structures (such as machine parts, airplane wings, engines) to locate defects, fractures, voids, among others, using noninvasive techniques so that the piece, if found intact, can be used in normal operation again. NDT is a crucially important field for monitoring the condition of expensive and critical equipment. Among other means used in NDT (such as optics and electromagnetic waves), ultrasound has the unique capability of penetrating deep into solids, which allows the detection of sub-surface defects. The advantages of cMUTs for other air applications (high dynamic range, efficiency, bandwidth, tolerance to heat, humidity, particles, and some chemicals) apply to air-coupled NDT as well. The dynamic range of cMUTs is sufficient to tolerate acoustical mismatch losses associated with going into solids from air and coming back. The targets

can be tested in pulse-echo configuration where a single transducer is used for both transmission and reception, or in a pitch-catch configuration, as shown in Fig. 22A. Fig. 22B and C show images obtained with two cMUTs in a pitch-catch configuration. The aluminum block is 30-mm thick, with an intentional dent on the backside. The dent is a 3 cm × 3 cm cross sign with a 0.5-mm depth [69].

Special applications

Structure health monitoring

The microstereolithography (MSL) technique has been used to construct polymeric capacitive transducer (PCT) manufacturing. This is a rapid prototyping technique that can be used to manufacture small components [45]. It uses the fact that thin layers of photosensitive polymers will solidify when illuminated with the correct wavelength and intensity of ultraviolet (UV) light. An object is constructed from a series of solidified layers, each of which can have a different form to give the required three-dimensional shape. Fig. 23 shows a schematic diagram of such a system. The object to be constructed is first designed in software as a series of layers. Fig. 24 shows how a cone would be constructed (the layers are shown at increased thickness for clarity). These layer patterns are fed to an illumination system whereby the required pattern is created via a series of micromirrors. The pattern is then used to illuminate a thin layer of liquid polymer next to a moveable build platform. This is slowly moved vertically so that, layer by layer, the object can be constructed from a set of individual layers.

In the case of a polymer cMUT, the construction method involved creating the back plate and membrane as two separate components, then applying the membrane to the depression in the back plate to form an air-filled gap [46]. The resulting polymer cMUT is shown schematically in Fig. 25 [70].

Operation of a PCT device

The devices fabricated using MSL have been evaluated for two different structural health-monitoring (SHM) applications. The first of these is acoustic emission. Here, signals emitted by a propagating crack, or some other defect, are detected using an array of sensors placed over an object. The time of arrival of the signal at each of the static sensors can be used to determine the location of the defect, and to reject other signals arising from outside the volume of interest. In addition, the waveform itself can give information about the event that generated it. A second area of SHM that has been investigated is the monitoring of vibrations of a structure, due to external excitation. This technique can be used, for instance, to check for changes in

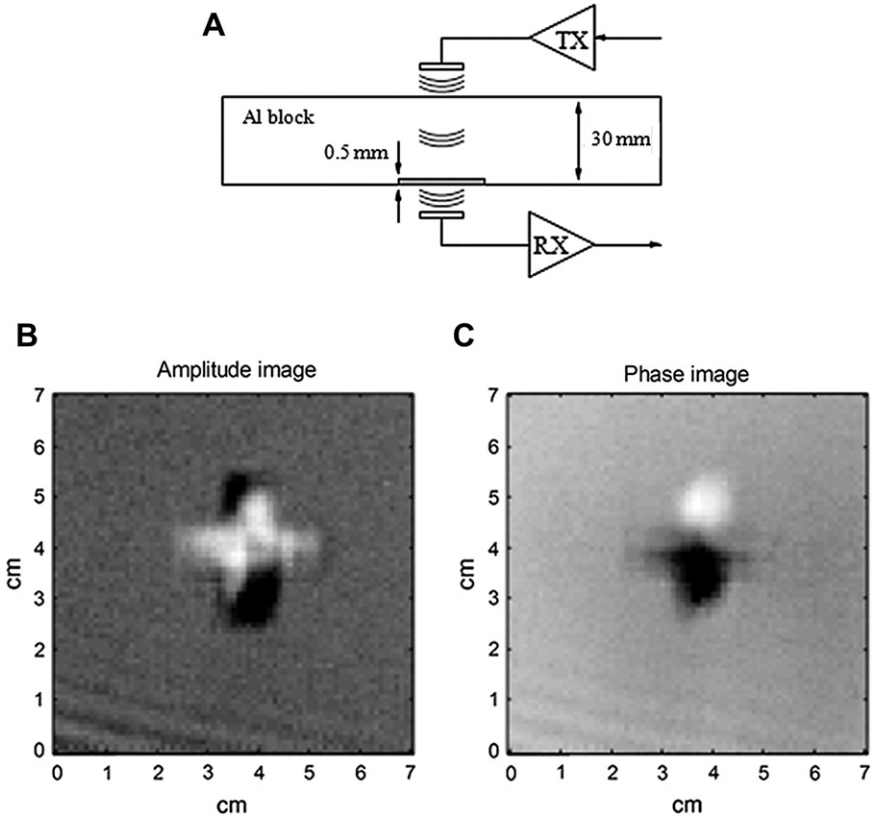

Fig. 22 (A) Experimental setup for through transmission experiment where the aluminum block is attached to a mechanical scanning stage; (B) through-transmission amplitude; and (C) phase images of the aluminum block using a single cMUT element at 2.3 MHz are plotted. The aluminum block is intentionally indented with a cross sign, which is 3 cm × 3 cm, and the line width is 5 mm. The indentation depth is only 0.5 mm. The images are gray-scale plots of the received raw signals, with no signal processing or beam shaping [69]. cMUT = capacitive micromachined ultrasonic transducer.

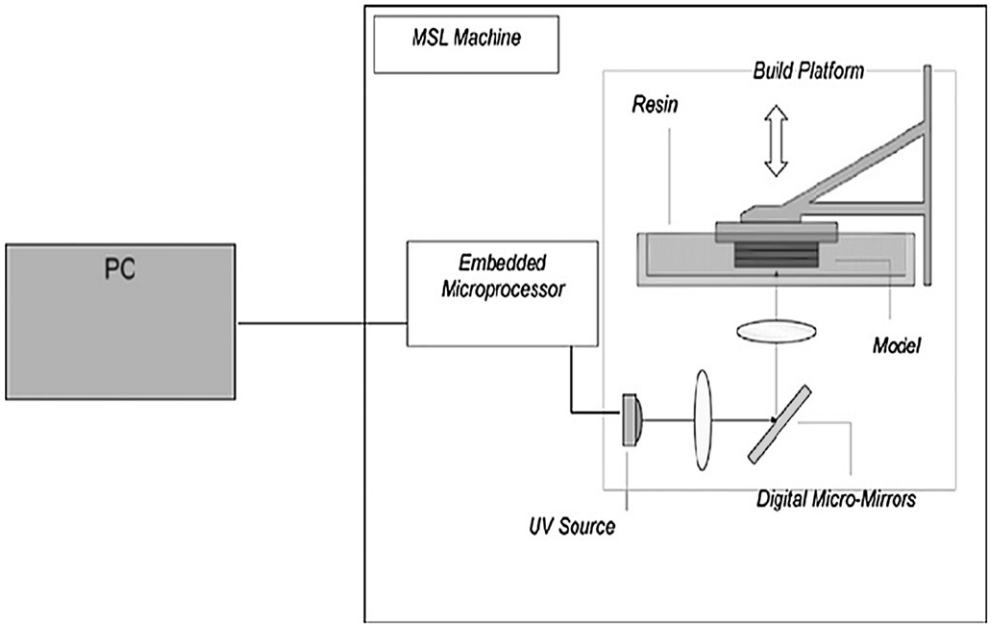

Fig. 23 Schematic diagram of an MSL system [70]. MSL = microstereolithography.

internal combustion engines, to monitor the wear of bearing surfaces, liquid flows in pipes, and many other applications. It was felt interesting to determine the usefulness of these new devices in both of these applications. Note that MEMS-type devices have been used for such monitoring, using a capacitive structure [47] fabricated via silicon processing (as in conventional cMUTs).

Detection of internal solid materials defects using Lamb waves

It was first necessary to determine that the devices could act as receivers of waves transmitted through a solid. There are a number of ultrasonic wave modes possible within solids following the process of acoustic emission from a defect. Within a plate-like structure, Lamb waves are the most commonly encountered guided wave mode, as they can propagate over long distances in plates and pipes [48]. They have been used for inspection and structural health monitoring in many situations [49]. The presence of Lamb waves can complicate the analysis of signals by their dispersive nature. When a source is excited by a broadband pulse, the different frequency components in a given dispersive Lamb mode will travel at different speeds, with more than one mode able to exist at any given frequency. At low frequency-thickness products, only the s_0 (symmetric) and a_0 (asymmetric) modes can propagate in a plate. The accurate determination of a particular mode of interest is extremely important, because each mode has different thickness values and is sensitive to different types of flaws. Fig. 26A and B shows the waveform received by

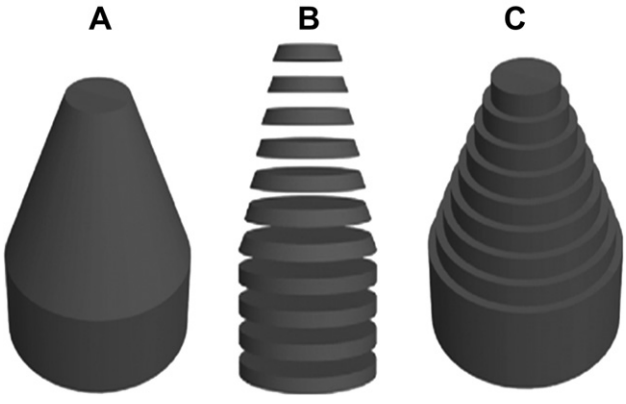

Fig. 24 Details of how (A) a cone would be constructed; from (B) a series of imaginary layers; to give (C) a real object that would result from such an MSL process. In practice, the layers would be sufficiently thin that individual steps would not be visible [70]. MSL = microstereolithography.

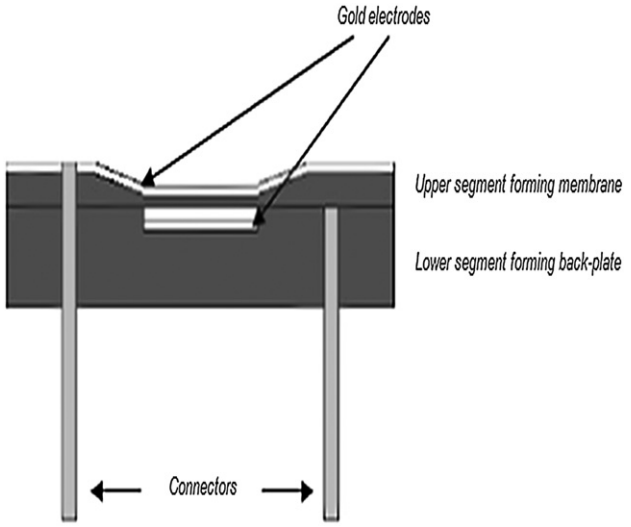

Fig. 25 A typical polymer CMUT as constructed using MSL techniques [70]. cMUT = capacitive micromachined ultrasonic transducer; MSL = microstereolithography.

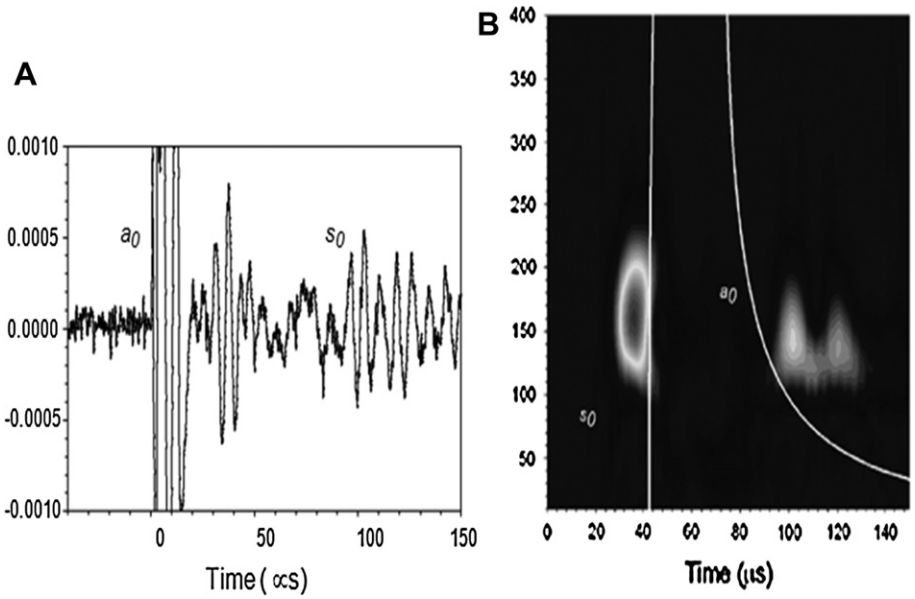

Fig. 26 Experimental results obtained using a piezoelectric a Panametrics contact transducer as a source and a polymer cMUT transducer, Coventry, UK as a receiver on a 2-mm-thick aluminum plate. (A) time waveform; (B) plot in the time-frequency domain, together with theoretical dispersion curves for the two zero order modes [70]. cMUT = capacitive micromachined ultrasonic transducer, Coventry, UK.

the MSL technique, using the piezoelectric transducer as the source of Lamb waves and excitation with a transient square-wave voltage waveform with a peak energy at 200 kHz, but with energy across a reasonable bandwidth.

Biometric recognition of human hand anatomic elements

Biometrics refers to methods for uniquely recognizing humans based upon one or more physical or behavioral traits. The first scientific method for biometric identification is commonly attributed to Alphonse Bertillon, a French criminal identification bureau chief in the late 1800s, who proposed an anthropometric method based on the measurement of the physical characteristics of the head, the bust, and the limbs of an individual [50]. This system was very popular at the end of the 19th century until it was supplanted by ink-based fingerprinting.

Although biometrics emerged from its extensive use in law enforcement to identify criminals, it is being increasingly used to establish person recognition in a large number of civilian applications. Nowadays, the applications of biometrics can be divided into the following three main groups:

- Commercial applications such as computer network logins, electronic data security, e-commerce, Internet access, automated teller machines, credit cards, physical access controls, cellular phones, personal digital assistants, medical records management, and distance learning
- Government applications such as a national identification card, correctional facilities, driver's licenses, social security, welfare disbursements, border control, and passport control;
- Forensic applications such as corpse identification, criminal investigation, terrorist identification, particularly DNA testing to determine parenthood, and specific iris recognition-based biometric technologies to locate and identify missing children and adults; and
- Hand geometry recognition is the longest implemented biometric type. Commercial hand geometry-based verification systems have been installed in hundreds of locations around the world. It simply measures and records length, width, thickness, and surface area of an individual's hand [51,52]. The geometry of the hand is not known to be very distinctive and hand geometry-based recognition systems cannot be scaled up for systems requiring identification of an individual from a large population. Hand geometry is exploited in conjunction with other biometric methods to improve recognition accuracy as well [53–55]. In general, several multimodal biometric systems, which use more than one independent source of information to recognize individuals, have been successfully developed in recent years [56–58].

Biometric technology and capability

The most commonly used technology in biometrics is the optical one, but other techniques (capacitive sensors [59], thermal near-infrared sensors [60], and, more recently, ultrasonic transducers [61]) have also been experimented with. Ultrasounds have some intrinsic advantages with respect to other methods; in fact, they are not sensitive to surface contaminations, such as stains, dirt, oil, or worn skin. In addition, they provide information not only of the skin surface; rather, they provide information for the entire volume under the investigated skin region. Furthermore, ultrasound detects liveness, and therefore can easily detect fakes.

Scanning acquisition time can be reduced using an ultrasonic linear array transducer that moves in a direction perpendicular to the electronic scanning plane. This technique is a 3-D ultrasound imaging modality with many possible biomedical applications [62—64] that can be extended to biometrics as well. The data are normally acquired by an ultrasound transducer and stored in a series of B-scans. The B-scans thus form a 3-D data set that can be visualized and processed in a large number of ways.

Iula and Santis [71] have achieved 3-D echographic images of different human hands based on the moving linear array technique to evaluate this technique for biometric recognition purposes.

The hands of several users were scanned and the corresponding 3-D matrices were built. The capability of the proposed technique to provide biometric information of the internal region of the hand was evaluated by analyzing several 2-D images (B-scan and C-scan). Figs. 27A and B show the B-scans of two different users at a scan depth of 41 mm. In Fig. 27, the blood flowing through some vessels is highlighted by the Doppler analysis to demonstrate the liveness in the investigated sample. The liveness check is usually required in several biometric authentication systems to detect fakes [65].

A comparison between Figs. 28A and B gives the first qualitative vision of the differences between the two ultrasonic images. In Fig. 28B, several possible internal elements are highlighted and possible quantitative parameters that could be exploited for biometric purposes are defined. These parameters include: the depth of each element from the skin (E_i), the height (EH_i) and the width (EW_i) of the elements, and the relative distances between two elements (DE_iE_j). For example, in the Fig. 28 the distance between two vessels (DV_2V_3) is highlighted in red; the tendon (TH_1, TW_1) and the muscle (MH_1, MW_1) dimensions in orange and green, respectively; the depth of the bone from the skin (B_i) in blue. All these parameters can be evaluated and measured to create a template of the user's characteristics in analogy with the enrolment and verification processes commonly used in classical 2-D hand geometry biometric systems [51,52,66,67].

To test the capability of the system to discriminate among different users, the hands of more than ten different people were analyzed. Fig. 28 shows the four more significant achieved B-scans. User A (Fig. 28A) is a man of medium weight; user B (Fig. 28B) is a man of medium weight who is thinner than A; user C (Fig. 28C) is a taller and more robust man than A and B; user D (Fig. 28D) is a small-sized woman. The images are obtained by setting a depth of 21 mm for all to maximize the resolution in the Z direction. In the plots, the measured values of some of the parameters defined above are shown.

3-D hand geometry technique

The proposed biometric characteristic has features similar to those of classical 2-D hand geometry, so researchers call it "3-D hand geometry." The conclusions of Iula and Santis' work [71], which is an experimental evaluation of the reliability of the moving linear ultrasonic array technique for biometric purposes, has been presented. Several B-scans were automatically acquired and stored by moving the probe in a direction orthogonal to the array, to form a 3-D matrix representing the under-skin volume.

B-scan and C-scan images of the palms of the hand of different users were analyzed and compared. The results show that, in the analyzed region (about 10 mm under the skin of the palm), there are several anatomic elements (including bones, bending tendons, muscle tissue, and blood vessels) that can be exploited for the measurement of biometric parameters. As matter of fact, a new biometric characteristic has been

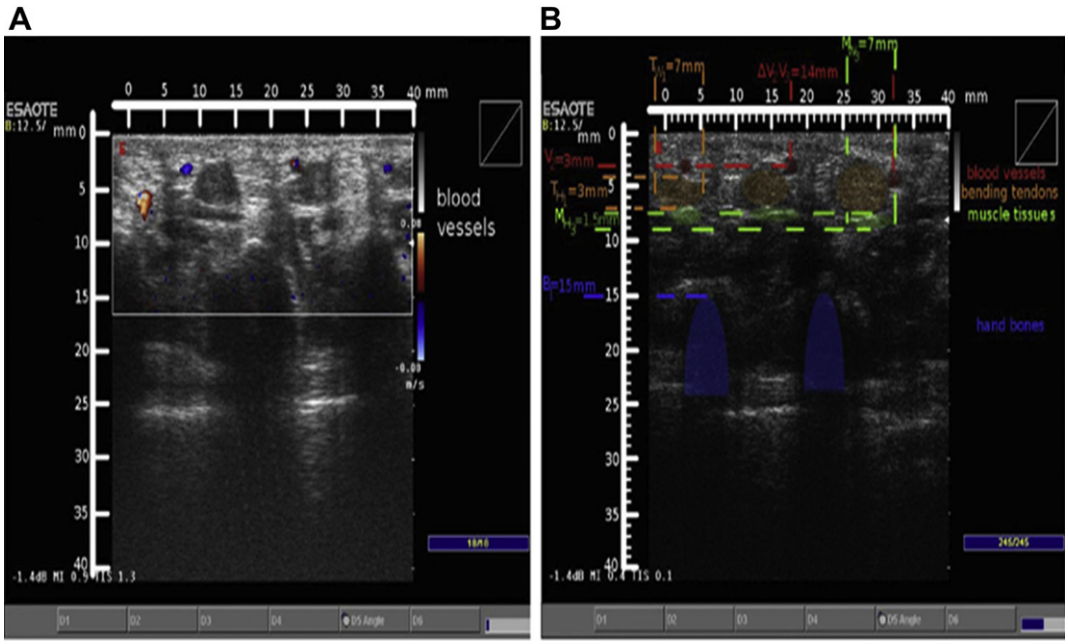

Fig. 27 B-scans of two different users at a scan depth of 41 mm. (A) Doppler analysis highlights blood flow; (B) definition of several possible biometric parameters [71].

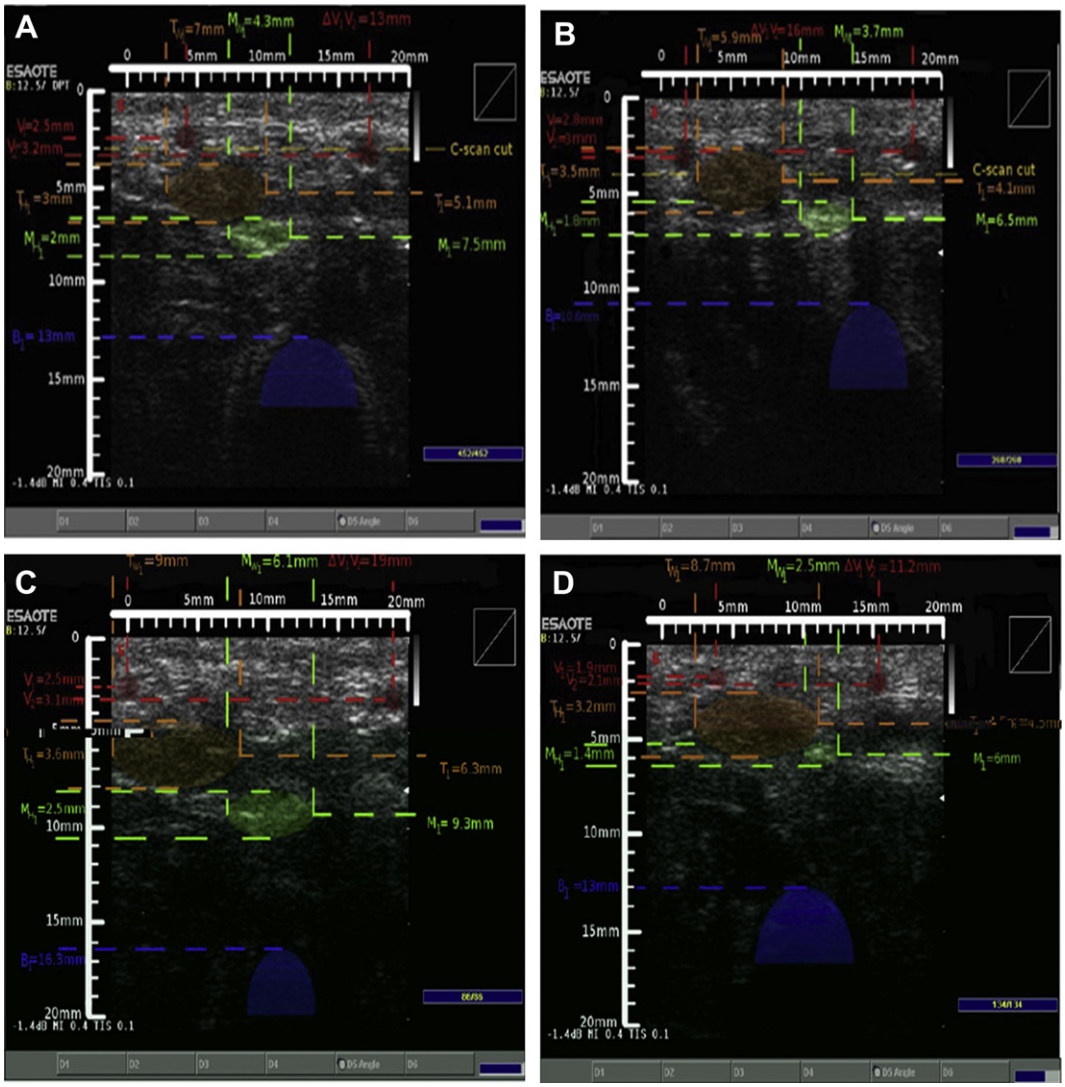

Fig. 28 B-scans from four different users. Some possible biometric parameters are quantified [71].

defined. The 3-D hand geometry has the same peculiar features, which seems very interesting for biometric purposes. First of all, 3-D geometry means that 3-D templates can be extracted for the enrolment procedures with an expected improvement of distinctiveness both for the increase of measurable parameters and for the possibility of recording 3-D patterns. Another important feature is the very low possibility of circumvention. In fact, it is very difficult to fake internal anatomic elements and, most importantly, the proposed technique can easily include a Liveness check by means of the Doppler analysis. Finally, 3-D hand geometry benefits the intrinsic characteristic of ultrasounds by making them not sensitive to skin contaminations or worn skin caused by fraudulent, environmental, or occupational reasons [71].

Ultrasonic characterization of blood coagulation

More than 50 factors may affect the blood coagulation mechanism, which makes it a complex physiologic process. The normal process of blood coagulation involves three essential steps. The first step is rupture of the vessel response or damage to the blood itself, which sets off a complex cascade of chemical reactions in the blood involving more than a dozen blood coagulation factors, the net result of which is the formation of a complex of activated substances collectively called prothrombin activator. Second, the prothrombin activator catalyzes the conversion of prothrombin into thrombin. Third, the thrombin acts as an enzyme to convert fibrinogen into fibrin fibers that enmesh platelets, blood cells, and plasma. Finally, the blood becomes a solid gel and a clot, which is composed of a meshwork of fibrin. Fibers running in all directions entrap blood cells, platelets, and plasma. All the essential steps require activated platelets, plasma cofactors, and Ca^{2+} [72].

Ultrasound-based methods that have been used to study blood coagulation properties have mainly employed measurements of acoustic parameters of clotting blood and ultrasound elastography. The measurement of backscattered ultrasound signals has been shown to vary according to the size, shape, concentration, density, and elastic properties of the scatters in a biologic tissue. The effect of fibrin fibers increases the size and changes the

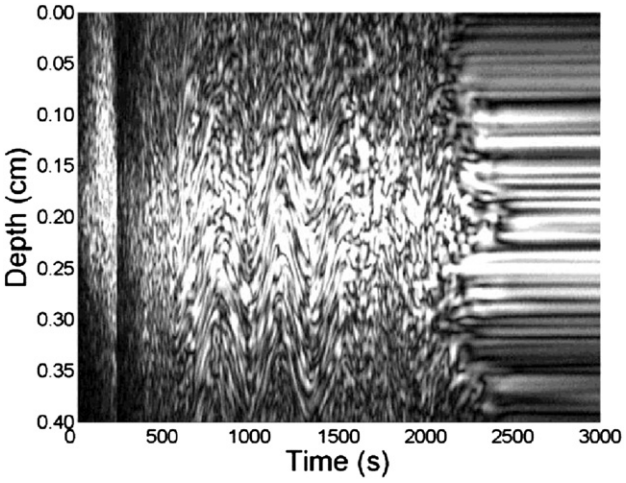

Fig. 29 A typical ultrasonic image during blood coagulation. The figure indicates that the formation of a clot with the blood becoming a solid gel results in the cessation of fluctuations in the ultrasonic scattering after approximately 2200 seconds [22,73].

shape of the scatters, which increases echogenicity during the clotting process [73,74]. Due to the turbulent motion of the fluid caused by fibrinogen converting into fibrin fibers, a fluctuation in backscattered signals during clotting is noted (Figs. 29 and 30). Many erythrocytes are trapped in the fibrin meshwork and the blood increases in viscosity, tending to become a solid gel, then the ultrasound attenuation increases (Fig. 31). This increase in attenuation could be due to an increase in viscosity and other frictional factors that consume energy, which is lost as heat.

The sound velocity changed because of the formation of fibrin fibers, which is inversely proportional to the square root of compressibility; and the compressibility of blood clots reduces due to the blood becoming stiffer [73]. Therefore, the increased sound velocity during clotting might be attributable to the variation of blood clot compressibility (Fig. 31). An analysis of the ultrasound parameters of the blood clots method could achieve the goals of real-time and continuous observation, since most of the acoustic properties associated with changes in tissue characteristics can be preserved without any loss of the original physiologic information. Because detailed variations of clotting can be detected by continuously monitoring the acoustic parameters, measuring the quantitative ultrasound parameters for assessing the blood coagulation process is suitable for laboratory examinations. Even though it is very difficult to obtain accurate values of these parameters *in vivo*, the obtained data could still have clinical relevance to human care because real-time ultrasound imaging has been shown to be a valuable tool for diagnosing intracranial hemorrhage and thromboses [72].

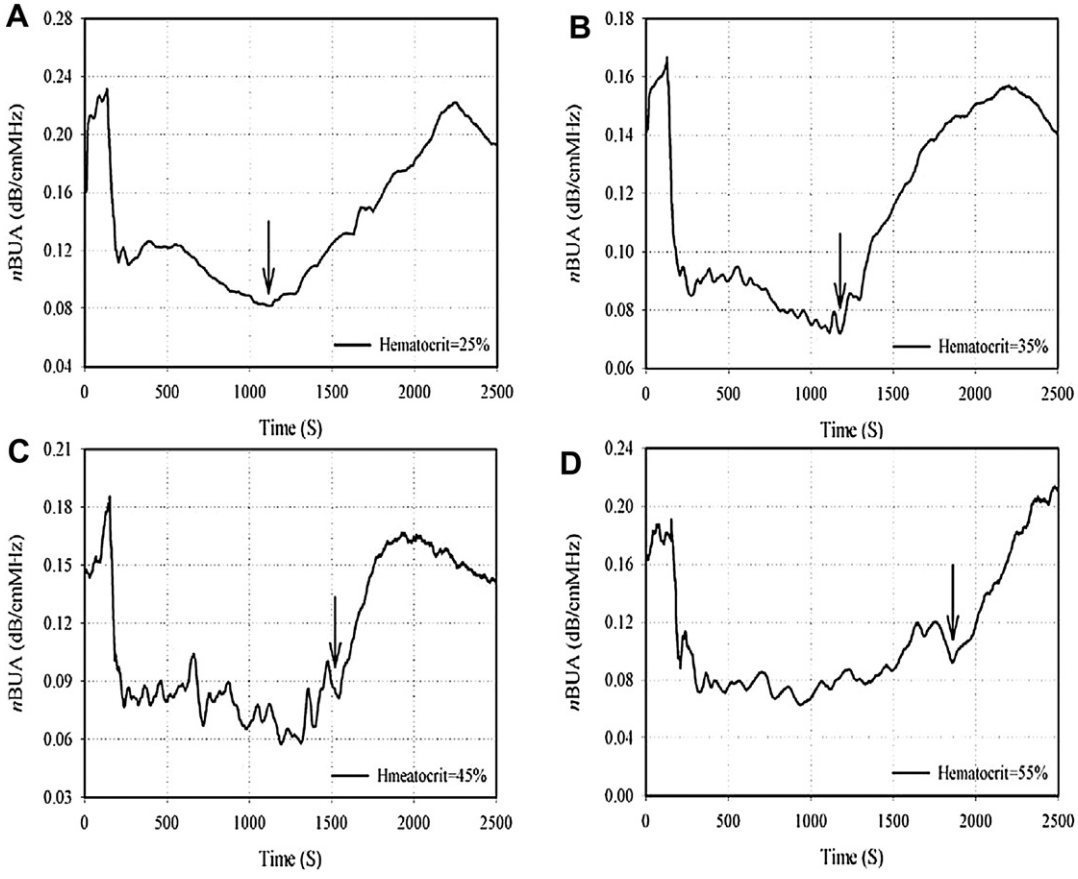

Fig. 30 normalized broadband ultrasonic attenuation (*nBUA*) as a function of time obtained from coagulating blood of (A) 25%; (B) 35%; (C) 45%; and (D) 55% hematocrit. The reaction time is indicated as an arrow symbol, which is defined as the *nBUA* to be dramatically increased. The coagulation time was increased with the increase of hematocrit [74].

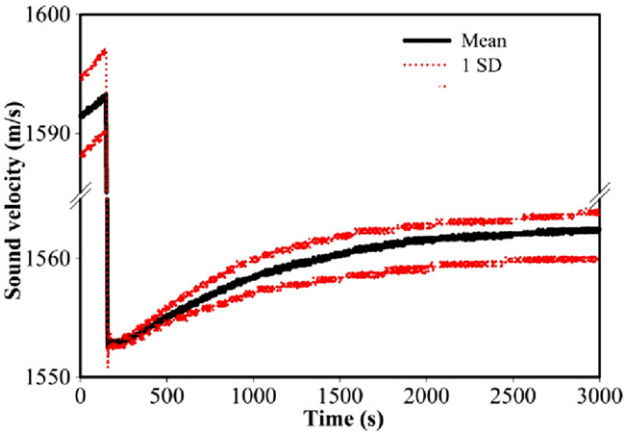

Fig. 31 Sound velocity as a function of time during blood coagulation and clot formation. The measurements were performed at 10 MHz ultrasound from porcine whole blood [73].

Conclusion

The history of cMUTs is now approaching two decades. From being an interesting and efficient air transducer, the cMUT is now considered as a major platform technology to realize many applications in industrial and medical diagnostic and therapeutic devices. In this paper, we described the basic principles of operation of cMUTs together with measurement results. We showed that we could predict the behavior of cMUTs beforehand and design for specific targets. This review paper also discusses recent fabrication technology. Modeling capabilities have improved enormously over the years and the potential of the technology has attracted many researchers into the field. As discussed above, cMUT technology offers many advantages over its competitor, piezoelectric transducer technology, both in air and immersion applications. The bandwidth in immersion applications implies significant improvements in medical imaging. cMUTs micromachining and integrated circuit technology make cMUTs the prime choice of ultrasonic transducer technology for many applications because of experience, scalability, batch production, electronic integration opportunities, and low manufacturing cost. The improvement of cMUTs technology based on increasing output pressure capability and reducing parasitic capacitance are two important issues. There is an expectation that a new generation of cMUTs will reach working frequencies of more than 20 MHz, providing improved image resolution. Finally, in this paper we discuss the advantages of polymer cMUTs, which can be made much more cheaply and simply than conventional silicon-based cMUTs, which require specialist silicon micromachining facilities. Furthermore, the polymer cMUT devices are good candidates for applications in Acoustic Emission (AE) and vibration monitoring.

References

[1] Hunt FV. The analysis of transduction, and its historical background: electroacoustics. 2nd ed. Cambridge, MA: Harvard University Press; 1982.
[2] Haller MI, Khuri-Yakub BT. A surface micromachined electrostatic ultrasonic air transducer. Ultrasonics Symposium IEEE 1994;2:1241—1244.
[3] Oralkan O, Ergun AS, Ching-hasiang C, et al. Volumetric imaging using 2D capacitive micromachined ultrasonic transducer arrays (CMUTs). Ultrasonic Symposium IEEE 2002;1083—1086.
[4] Cheng CH, Ergun AS, Khuri-Yakuub BT. Electrical through-wafer interconnects with sub-picofarad parasitic capacitance. Microelectromechanical Systems Conference IEEE 2001;18—21.
[5] Averkiou MA, Roundhill DN, Powers JE. A new imaging technique based on the nonlinear properties of tissues. Ultrasonic Symposium IEEE 1997;1561—1566.
[6] Hansen ST, Mossawir BJ, Ergun AS, et al. Air-coupled nondestructive evaluation using micromachined ultrasonic transducers. Ultrasonic Symposium IEEE 1999;1037—1040.
[7] Cittadine A, Nystrom J. MEMS-finally ready for prime time using micro sensors and a newly developed ASIC for small-diameter pipe ultrasonic metering. Flow Control Mag 2001;8:231—45.
[8] Hansen ST, Ergun AS, Khuri-Yakub BT. Improved modeling and design of microphones using radio frequency detection with capacitive micromachined ultrasonic transducers. Ultrasonic Symposium IEEE 2001;961—964.
[9] Yaralioglu GG, Badi MH, Ergun AS, et al. Lamb wave devices using capacitive micromachined ultrasonic transducers. Appl Phys Lett; 2001:111—3.
[10] Jagannathan H, Yaralioglu GG, Ergun AS, et al. Micro-fluidic channels with integrated ultrasonic transducers. Ultrasonic Symposium IEEE 2001;859—862.
[11] Ladabaum I, Xuecheng J, Atalar HT, et al. Surface micromachined capacitive ultrasonic transducers. IEEE Transactions on Ultrasonics, Ferroelectrics, and Frequency Control 1998; 678—690.
[12] Timoshenko S, Woinowsky-Krieger S. Theory of plates and shells. 2nd ed. USA: McGraw-Hill Book Company Inc; 1959.
[13] Lee YS, Wise KD. A batch-fabricated silicon pressure capacitive transducer with low temperature sensitivity. IEEE Trans Electron Devices 1982;29:42—8.
[14] Rafiq M, Wykes C. The performance of capacitive ultrasonic transducers using V-grooved backplates. Measure Sci Tech 1991;2:168—74.
[15] Carr H, Wykes C. Diagnostic measurements in capacitance transducers, 31. Ultrasonic Elsevier; 1993. pp. 13—20.
[16] Mattila P, Tsuzuki F, Vaataja H, et al. Electroacoustic model for electrostatic ultrasonic transducers with V-grooved backplates. *IEEE Trans. Ultrason., Ferroelectr., Freq. Control* 1995;42:1—7.
[17] Schindel DW, Hutchins DA, Zou L, et al. The design and characterization of micromachined air-coupled capacitance transducers. *IEEE Trans. Ultrason., Ferroelectr., Freq. Control* 1995;42:42—50.
[18] Suzuki K, Higuchi K, Tanigawa HA. Silicon electrostatic ultrasonic transducer. *IEEE Trans. Ultrason., Ferroelectr., Freq. Control* 1989;36:620—7.
[19] Caliano G, Foglietti V, Cianci E, et al. A silicon microfabricated electrostatic transducer: 1 MHz transmission in air and in water. Microelect Eng Sci Direct 2000;53:573—6.
[20] Noble RA, Jones ADR, Robertson TJ, et al. Novel, wide bandwidth, micromachined ultrasonic transducers. *IEEE Trans. Ultrason., Ferroelectr., Freq. Control* 2001;48:1495—507.
[21] Eccardt PC, Niederer K. Micromachined ultrasound transducers with improved coupling factors from CMOS compatible process. Ultrasonics 2000;38:774—80.
[22] Huang Y, Ergun AS, Haeggstrom E, et al. Fabricating capacitive micromachined ultrasonic transducers with wafer-bonding technology. J Microelectromechan Sys 2003;12:128—37.
[23] Mastrangelo CH, Hsu CH. Mechanical stability and adhesion of microstructures under capillary forces — part I, basic theory. J Microelectromechan Sys 1993;2:33—43.

[24] Ladabaum I, Jin X, Soh HT, et al. Microfabricated ultrasonic transducers: towards robust models and immersion devices. Ultrasonic Symposium IEEE 1996;1:335—338.
[25] Jin XC, Ladabaum I, Degertekin FL. Fabrication and characterization of surface micromachined capacitive ultrasonic immersion transducers. J Microelectromechan Sys 1999;8:100—14.
[26] Jin XC, Ladabaum I, Khuri-Yakub BT. Surface micromachined capacitive ultrasonic immersion transducers. IEEE Microelectromechan Sys; 1998:649—54.
[27] Calmes S, Cheng CH, Degertekin FL, et al. Highly integrated 2-D capacitive micromachined ultrasonic transducers. Ultrasonic Symposium IEEE 1999;2:1163—1166.
[28] Memmi D, Foglietti V, Cianci E, et al. Fabrication of micromechanical capacitive ultrasonic transducers by low temperature process. Sensor Actuator A: Phys 2002;99:85—91.
[29] Cianci E, Visigalli L, Foglietti V, et al. Improvements towards a reliable fabrication process for CMUT. Microelectron Eng 2003;67—68:602—8.
[30] Stoffel A, Kovacs A, Kronast W, et al. LPCVD against PECVD for micromechanical applications. J Micromechan Microeng 1996; 6:1—13.
[31] Cianci E, Minotti A, Foglietti V, et al. One-dimensional capacitative micromachined ultrasonic transducer arrays for echo graphic probes. Microelectron Eng 2004;73—74:502—7.
[32] Martin Abreu JM, Calderon L, Ceres R, et al. Shaping the detection lobe of ultrasonic ranging devices. Measure Sci Technol 1997;8:1279—84.
[33] Borenstein J, Koren Y. Obstacle avoidance with ultrasonic sensors. IEEE J Robotic Automat 1988;4:213—8.
[34] Folkestad T, Mylvaganam KS. Chirp excitation of ultrasonic probes and algorithm for filtering transit times in high-rangeability. Gas flow metering. *IEEE Trans. Ultrason., Ferroelectr., Freq. Control* 1993;40:193—215.
[35] Ergun AS, Yaralioglu GG, Khuri-Yakub BT. Capacitive micromachined ultrasonic transducers: theory and technology. J Aerospace Eng 2003;16:76—84.
[36] Nygaard G, Mylvaganam S, Engan HE. Integration of impedance measurements with transit time measurements for ultrasonic gas mass flow metering-model and experiments with transducers in different vibration modes. Ultrasonics Symposium IEEE 2000;1:475—482.
[37] Huang Y, Haeggstorm EO, Zhuang X, et al. Optimized membrane configuration improves cMUT performance. Ultrasonic Symposium IEEE 2004;1:505—508.
[38] Oralkan O, Hansen ST, Bayram B, et al. High frequency Cmut arrays for high-resolution medical imaging. Ultrasonics Symposium IEEE 2004;1:399—402.
[39] Oralkan O, Hansen ST, Bayram B, et al. Cmut ring arrays for forward-looking intravascular imaging. Ultrasonic Symposium IEEE 2004;1:403—406.
[40] Bayram B, Haegstrom E, Yaralioglu GG, et al. A new regime for operating capacitive micromachined ultrasonic transducers. *IEEE Trans. Ultrason., Ferroelectr., Freq. Control* 2003;50: 1184—90.
[41] Bayram B, Oralkan O, Ergun AS, et al. Capacitive micromachined ultrasonic transducer design for high power transmission. *IEEE Trans. Ultrason., Ferroelectr., Freq. Control* 2005;52:326—39.
[42] Oralkan O, Bayram B, Yaralioglu GG, et al. Experimental characterization of collapse-mode operation of capacitive micromachined ultrasonic transducers. *IEEE Trans. Ultrason., Ferroelectr., Freq. Control* 2006;53:1513—23.
[43] Oralkan O, Ergun AS, Ching-Hsiang C, et al. Volumetric ultrasound imaging using 2-D CMUT arrays. *IEEE Trans. Ultrason., Ferroelectr., Freq. Control* 2003;50:1581—94.
[44] Demirci U, Ergun AS, Oralkan O, et al. Forward-viewing CMUT arrays for medical imaging. *IEEE Trans. Ultrason., Ferroelectr., Freq. Control* 2004;51:886—94.
[45] Varadan VK, Jiang X, Varadan VV. Microstereolithography and other fabrication techniques for 3D MEMS. New York: John Wiley & Sons; 2001. p. 260.
[46] Hutchins DA, Billson DR, Bradley RJ. Polymer-based CMUTS. XX: 19th International Congress on Acoustics (ICA 2007); 2007. 38.
[47] Ozevin D, Greve DW, Oppenheim IJ, et al. Resonant capacitive MEMS acoustic emission transducers. Smart Mat Struct 2006; 15:1863—71.
[48] Viktorov IA. Rayleigh and lamb waves: physical theory and application. NY: Plenum; 1967.
[49] Kessler SS, Dunn CT. Optimization of lamb wave actuating and sensing materials for health monitoring of composite structures. 10th International Symposium on Smart Structures and Materials, San Diego, CA; 2003:123—33.
[50] Henry TF, Rhodes AB. Optimization of lamb wave actuating and sensing materials for health monitoring of composite structures. New York: Abelard-Schuman; 1956.
[51] Ross A, Jain AK, Pankanti SA. Prototype hand geometry-based verification system. 2nd International Conference on Audio- and Video-based Biometric Person Authentication (AVBPA) Washington D.C.; 1999. pp.166—171.
[52] Zunkel RL. Hand geometry based verification, biometrics. Springer; 1999.
[53] Kumar A, Wong DCM, Shen HC, et al. Personal verification using palm print and hand geometry biometric. AVBPA; 2003: 668—75.
[54] Kumar A, Zhang D. Combining fingerprint, palm print and hand-shape for user authentication. International Conference on Pattern Recognition ICPR; 2006: 549—552.
[55] Shahin MK, Badawi AM, Rasmy ME. A multimodal hand vein, hand geometry and fingerprint prototype design for high security biometrics. Egypt: Cairo International Biomedical Engineering Conference on CIBEC; 2008: 1—6.
[56] Ross A, Jain AK. Multimodal biometrics: an overview. 12th European Signal Processing Conference on EUSIPCO; 2004. pp. 1221—1224.
[57] Ross Jain AK. Information fusion in biometrics. Patt Recog Lett Elsevier Science B.V., 2003;24:2115—25.
[58] Sadowitz M, Latifi S, Walker D. An overview of iris and retina scans and their fusion in a biometric system. International Conference on Image Processing, Computer Vision and Pattern Recognition IPCV; Las Vegas Nevada, USA, 2008: 119—123.
[59] Lee JW, Min DJ, Kim J, et al. A 600-dpi capacitive fingerprint sensor chip and image-synthesis technique. IEEE J Solid-State Circuits 1999;34:469—75.
[60] Wang L, Leedham G. A thermal hand vein pattern verification system. Lect Notes Comp Sci 2005;3687:58—65.
[61] Maev RG, Bakulin EY, Maeva EY, et al. High resolution ultrasonic method for 3D fingerprint representation in biometrics. 29th International Symposium on Acoustical Imaging. Shonan Village, Kanagawa, Japan; 2007.
[62] Fenster A, Downey DB, Cardinal HN. Three-dimensional ultrasound imaging. Phys Med Biol 2001;46:R67—99.
[63] Gee A, Prager R, Treece G, et al. Engineering a freehand 3D ultrasound system. Patt Recog Lett 2003;24:757—77.
[64] Hossack JA, Sumanaweera TS, Napel S, et al. Quantitative 3-D diagnostic ultrasound imaging using a modified transducer array and an automated tracking technique. IEEE Transactions on Ultrasonics, Ferroelectrics, and Frequency Control 2002; 49:1029—38.
[65] Abhyankar A, Schuckers S. Fingerprint liveness detection using local ridge frequencies and multi resolution texture analysis techniques. IEEE International Conference on Image Processing; 2006: 321—324.
[66] Varchol P, Levicky D. Using of hand geometry in biometric security systems. Radio Eng 2007;16:82—7.

[67] Jain AK, Ross A, Uludag U. Biometric template security: challenges and solutions. European Signal Processing Conference on EUSIPCO; 2005.
[68] Cianci E, Foglietti V, Minotti A, et al. Fabrication techniques in micromachined capacitive ultrasonic transducers and their applications. MEMS/NEMS; 2006:353—82.
[69] Ergun AS, Yaralioglu GG, Oralkan O. MEMS/NEMS techniques and applications of capacitive micromachined ultrasonic transducers. MEMS/NEMS; 2006:553—615.
[70] Hutchins DA, Billson DR, Bradley RJ, et al. Structural health monitoring using polymer-based capacitive micromachined ultrasonic transducers (CMUTs). Ultrasonics 2011;51:870—7.
[71] Iula A, De Santis M. Experimental evaluation of an ultrasound technique for the biometric recognition of human hand anatomic elements. Ultrasonics 2011;51:683—8.
[72] Huang C-C, Lin Y-H, Liu T-Y, et al. Review: study of the blood coagulation by ultrasound. J Medi Biologic Eng 2011;31:79—86.
[73] Huang CC, Wang SH, Tsui PH. Detection of blood coagulation and clot formation using quantitative ultrasonic parameters. Ultrasound Med Biol 2005;31:1567—73.
[74] Huang CC, Wang SH. Characterization of blood properties from coagulating blood of different hematocrits using ultrasonic backscatter and attenuation. Jap J Appl Phys 2006;54: 7191—6.